Chemical and Biological Synthesis of Fe_3O_4 Nanoparticle and its Application for Removal of Methylene Blue from Aqueous Solution

KENENI DEBELU

A Thesis Submitted to the Department of Applied Chemistry

School of Applied Natural Science

In partial fulfillment of the Requirements for the Degree of Master of Science in Applied Chemistry (Industrial Chemistry)

Office of Post Graduate Studies

Adama Science and Technology University (ASTU)

September, 2022

Adama, Ethiopia

Chemical and Biological Synthesis of Fe_3O_4 Nanoparticle and its Application for Methylene Blue Removal from Aqueous Solution

KENENI DEBELU

ADVISOR: DEREJE TSEGAYE (PhD)

CO-ADVISOR: FEDLU KEDIR (PhD)

Thesis Submitted to the Department of Applied Chemistry

School of Applied Natural Science

In partial fulfillment of the Requirements for the Degree of Master of Science in Chemistry (Industrial Chemistry)

Office of Post Graduate Studies

Adama Science and Technology University

Sebtember, 2022

Adama, Ethiopia

DECLARATION

I hereby declare that this M.Sc. thesis entitled **"Chemical and Biological Synthesis of Fe_3O_4 Nanoparticle and its Application for Methylene Blue Removal from Aqueous Solution"** is my original work and has not been presented for a degree in any other university and all sources of material used for this thesis has been duly acknowledged through citation

KENENI DEBELU _____ _____

Name of student Signature Date

RECOMMENDATION OF ADVISORS/ SUPERVISORS

I/we, the advisor of this thesis, hereby certify that I/we have read the revised version of the thesis entitled **"Chemical and Biological Synthesis of Fe_3O_4 Nanoparticle and its Application for Methylene Blue Removal from Aqueous Solution"** by Keneni Debelu submitted in partial fulfillment of the requirements for the degree of Masters of Science in applied chemistry (Industrial chemistry). Therefore, I/we recommend the submission of a revised version of the thesis to the department following the applicable procedures.

_____	_____	_____
Major Advisor	Signature	Date
_____	_____	_____
Co- advisor	Signature	Date

APPROVAL PAGE

I/we, the advisors of the thesis entitled **"Chemical and Biological Synthesis of Fe_3O_4 Nanoparticle and its Application for Methylene Blue Removal from Aqueous Solution"** and developed by Keneni Debelu hereby certify that the recommendation and suggestions made by the board of examiners are appropriately incorporated into the final version of the thesis.

_____	_____	_____
Major Advisor	Signature	Date
_____	_____	_____
Co-advisor	Signature	Date

APPROVAL OF BOARD OF REVIEWERS

We, the undersigned, members of the Board of Examiners of the thesis by Keneni Debelu have read and evaluated the thesis entitled **"Chemical and Biological Synthesis of Fe_3O_4 Nanoparticle and its Application for Methylene Blue Removal from Aqueous Solution"** and examined the candidate during the open defense. This is, therefore, to certify that the thesis is accepted for partial fulfillment of the requirement of the degree of Master of Science in Industrial chemistry.

_____	_____	_____
Chairperson	Signature	Date
_____	_____	_____
Internal Examiner	Signature	Date
_____	_____	_____
External Examiner	Signature	Date

Final approval and acceptance of the thesis are contingent upon the submission of its final copy to the Office of Postgraduate Studies (OPGS) through the Department Graduate Council (DGC) and School Graduate Committee (SGC).

_____	_____	_____
Department Head	Signature	Date
_____	_____	_____
School Dean	Signature	Date
_____	_____	_____
Office of Postgraduate Studies, Dean	Signature	Date

ACKNOWLEDGEMENTS

First and foremost, I would like to thank the Almighty God and his mother St. Marry for giving me the health, strength, wisdom, and patience to complete this thesis. Then I would like to give my honorable thanks to Adama Science and Technology University as a whole for allowing me an opportunity to do this research thesis. My thanks also go to all school of applied natural sscince (SoANS) and the Department of applied chemistry to give me this chance. Next, I would like to express my deep gratitude and greatest thanks to my advisor Dr. Dereje Tsegaye for his cooperation, suggestions, supervision and remarks, appreciable encouragement, fatherly consultation, and taking his time to read and correct my document, starting from the proposal writing to the completion of this thesis.

Although I would like to express my genuine heartfelt gratitude to my Co-adviser Dr. Fedlu Kedir for his valuable suggestion, comments, corrections, and professional & technical guidance throughout my work for the successful accomplishment of this thesis proposal. I would like to appreciate my colleagues, Analytical Chemistry Laboratory Technicians, Department of Applied Chemistry, Department of Chemical Engineering, Department of Applied Biology, Department of Material Engineering, and all individuals who supported me by sharing ideas or offering materials support which is an input for this work.

Finally, I would like to thank all my beloved family and my entire friends who stood beside me through the difficult times.

TABLE OF CONTENTS

Contents Pages

LIST OF TABLES

TABLES PAGES

LIST OF FIGURES

FIGURES PAGES

LIST OF ABBREVIATIONS

ASTU	Adama science and technology university
BOD	Biological oxygen demand
COD	Chemical oxygen demand
DTA	Differential thermal analysis
FT-IR	Fourier transforms infrared spectroscopy
FWHM	Full Width at Half Maximum
IONPs	Iron oxide nanoparticles
MB	Methylene blue
MNPs	Mono nanoparticles
MRI	Magnetic resonance imagining
PJLE	Prosopis juliflora leaf extract
ROSs	Reactive oxygen species
SEM	Scanning electron microscopy
TEM	Transmission electron microscopy
TGA	Thermo-gravimetric analysis
UV-Vis	UV-visible spectroscopy
XRD	X-ray diffraction

ABSTRACT

The application of greenly and chemically synthesized iron oxide (magnetite) nano particles for the removal of methylene blue from an aqueous solution is what was studied in this thesis. The XRD, FT-IR, UV-Visible spectroscopy and SEM results reveal that a chemical and greenly synthesized iron nano particle with a different size was synthesized using Prosopis Juliflora leaf extract and ferric and ferrous chloride salt precursors. The average crystal ssize of the synthesized NPs was calculated using the Debye-Scherer equation. The average crystal size of magnetite NPs was found 16nm (1:1 ratio), 19nm (1:2 ratio), 14nm (2:1 ratio) and 12nm(chemical mwthod). FTIR spectrum of magnetite NPs showed the intraction between the functional groups and phytochemical in the Prosopis julifera leaves extract and magnetite NPs. The deployment of greenly synthesized iron oxide nanoparticle (GInP) in the removal of methylene blue was studied after this diminutive GInP had been procreated by reduction of ferric iron in presence of P. juliflora leaf extract and coprecipitation for chemical method. The methylene blue dye removal capability of both GInP and chemically synthesized iron oxide nanoparticles was investigated for methylene blue concentrations ranging from 10 ppm - 50 ppm in both methods. Batch adsorption experiments were performed to investigate the influence of pH, contact time, adsorbent dosage, and initial concentration. A maximum methylene blue percentage of 99.75 and 99.505 in the green and chemical methods were observed, respectively at pH 9 for 10 ppm MB concentration in 60 min using 0.5 g of adsorbent dosage. The adsorption kinetics data were well fitted with the pseudo-second-order rate model with high regression coefficient (0.9986 and 0.9973) in the green and chemical method, respectively. The methylene blue removal process was found to be well fitted with the Freundlich isotherm model with determination coefficients valeu of 0.9981 and 0.9836 in the green and chemical methods, respectively. Reusability was also studied by using one sample with 0.5 g for five cycles and up to 84.6% and 83.9% by green and chemical method, respectively of methylene blue can be removed. It has been found that greenly synthesized magnetite nano particle show high selectivity and adsorption capacities for the removal of methylene blue dye from an aqueous solution.

***Keywords**: Iron oxide nano particle, adsorption, methylene blue, green synthesis, leaf extract*

CHAPTER ONE

1. INTRODUCTION

1.1. Background of the Study

Nanotechnology can be defined as the manipulation of matter through certain chemical and physical processes to create materials with specific properties, which can be used in particular applications. The main advantage of using nanoparticles compared to conventional material is the high surface area for the development of chemical reactions, physical interchange, etc. In addition to that, nanomaterials effectively remove contaminants even at low concentrations, to generate less waste post-treatment and novel reactions take place at the nanometric scale due to the increase in the number of active sites (Pradeep.T, 2009). Nanoparticles themselves can interfere with many tests, and it is often necessary to adapt the protocol to obtain reliable results (Djurisic et al., 2015). The scarcity of water is a major concern in today's world. The scarcity of water is due to rapid population growth, increased industrialization, and decreased amounts of rainfall in the previous decades. Water pollution by untreated synthetic dye effluents released from industries has been identified as one of the consequences of the worsening situation of water scarcity in society (Tuli et al., 2020). The rapid urbanization of natural resources and the increase in the number of industries, especially textile industries are posing a threat to the water bodies by discharging contaminated wastewater. These discharge effluents contain various harmful and toxic components, heavy metals, BOD, COD, and also dyes. This deteriorates the quality as well as quantity of water and makes it unsafe for further use (Kheddo, Rhyman, Elzagheid, Jeetah, & Ramasami, 2020; Yagub, Sen, Afroze, & Ang, 2014).

A dye is a chemical compound that is used as a colored substance that binds to the substrate to which it is being applied. Nowadays, dyes are broadly used in many industries including textiles, paper, plastic, rubber, automotive, trucking, marine industries, food industries, paint industries, coating, etc. They have generally an artificial starting place and a complicated structure that makes them persistent to light, oxidation, and biodegradable processes. The aqueous solution contains a very large amount of unused dye particles and other chemicals released to the water

bodies generated from the various industries which pose a great risk to the aquatic atmosphere (Sarkar et al. 2020), alongside consuming oxygen and elevating biochemical oxygen demand. Water pollution has become a global issue causing unbalanced biodiversity and affecting human health by affecting more than 40% of the global population. About 80% of it is due to human activities and the coloring industry. Many methods have been developed such as coagulation-flocculation (García-Montaño et al. 2008), aero-big anaerobic treatment (Hussein Koupaie et al. 2011), membrane filtration (AlventosadeLara et al. 2012), and adsorption technique (Zhang et al. 2014) for the removal of the dye. However, the surface phenomenon of adsorption is found to be one of the most effective ways to remove pollutants such as dyes from water (Surendhiran et al. 2017). In general, dye manufacturers normally use activated carbon as an adsorbent for the adsorption of dyes due to its high porosity and surface vicinity of approximately 500 to 2000 m^2/g (Carrott et al. 1991), but activated carbon requires controlled pressure generation and regeneration. Furthermore, activated carbon must be regenerated at regular intervals of time, making it highly expensive and inefficient for use in industries. Presently, adsorbents based on nanoparticles have shown great performance in the removal of dyes from the aqueous solution because of their exceptional physical and chemical properties such as high surface area, nanoscale size, and chemical composition. In addition, these nanoparticles allow modification of their surfaces by the introduction of certain organic ligands and groups, which increase the adsorption parameters considerably (Marcelo et al. 2020).

As a result, there is a need to synthesize such absorbents with proper particle sizes for the removal of dyes in wastewater. Up to now, several methods can be used to synthesize iron-oxide nanomaterials. These methods include chemical methods (such as hydrothermal synthesis, thermal decomposition, co-precipitation, sol-gel method, physical method, and green synthesis method (such as plant extract, fungi, bacteria, and yeast) (Zuolian Cheng *et al*, 2012). Biosynthesis of iron-oxide nanoparticles could be an alternative to traditional chemical methods for the production of metallic nanomaterials in a clean, non-toxic, and ecologically sound manner (Ahmad et al., 2011). Moreover, in green synthesis processes, there is no need to use high pressure, energy, temperature, and toxic chemicals. Plant-mediated biological synthesis of nanoparticles has gained importance only in recent years.

Synthesis of nanoparticles using plants provides more biocompatible nanoparticles than chemical synthesis, whereas chemical synthesis may lead to the presence of some toxic chemical species on the surface of the nanoparticles that may have undesirable effects in biomedical applications. Chemical approaches may be harmful to humans and impose environmental and health risks. In another approach, magnetic nanoparticles are produced by biological resources (biosynthesis or green synthesis).

In this study, the leaf extracts of P. *julifera* was used for the green synthesis of ecofriendly Fe_3O_4 nanoparticle for the removal methylene blue of from an aqueous solution. Here, the aim was to evaluate the removal of dyes by magnetite Fe_3O_4 nanoparticles that were synthesized both by the chemical and green methods for the removal of methylene blue removal from waste water. This would also be compared with Fe_3O_4 nanoparticle that was synthesized by a chemical method for the same application. The synthesized materials were also characterized by TGA-DTA, X-ray diffraction (XRD), UV-Visible spectroscopy, Fourier Transform Infrared Spectroscopy (FI-IR), and scanning electron microscopy (SEM) techniques.

1.2. Statement of the Problem

Water is one of the most important resources for sustainable development and core for socio-economic development, healthy ecosystems, survival of humans, and living organisms. But, the fast growth of industrial activities especially textile industries ends in the generation of organic pollutants that contain organic dyes like methylene blue dye, phenols, and other persistent organic pollutants. Discharging of these organic pollutants can cause serious problems, to the environment and human health due to their carcinogenicity (Bruno Lellis et al, 2019). The efficient removal of these pollutants from industrial wastewater makes the environment safe for a living organisms. The main sources of irrigation water in the city of Ethiopia are polluted and untreated wastewater that contains different pollutants including methylene blue (MB). Removal of organic dyes from wastewater is one of the environmental challenges and a public health matter. Azo dyes like methylene blue (MB) are the most important sources of textile dyes utilized in industrial applications. Removal of MB dye by conventional treatment methods is difficult due to its stability and non-biodegradable nature. Hence, different physicochemical methods were developed for removing dyes from wastewater but it's not sufficient for the

elimination of those dyes (Karthik, V et al., 2020). Wastewater containing dyes is undesirable since a tiny amount of dye material destroys the aesthetic values of water. It is necessary to effectively treat effluent-containing dyes due to the environmental and toxicological threats posed to humans and aquatics. There are different methods for the removal of dyes from wastewater effluents. The conventional methods can be categorized as biological, chemical, and physical methods (Yuan et al., 2019). The biological treatment methods include activated sludge, trickling filters, anaerobic process, and oxidation ponding; which have the advantage of eco-friendly nature, minimum usage of chemicals, and energy saving but these methods are not effective for treating dyestuff wastewater because many commercial dyestuffs are toxic to micro-organisms being used in the treatment process. Biological treatment methods also require a large land area and minimum flexibility in design and operation (Karthik, Saravanan, Bharathi, Dharanya, & Meiaraj, 2014). Coagulation-flocculation, chemical precipitation, ion exchange, and ozone oxidation belong to the group of chemical treatment methods, and dyes can be removed completely by this method. However, these methods have the limitations of high energy demand, large consumption of chemical reagents, high cost, and require additional treatment before disposal (Monika, 2012). Physical treatment of wastewater includes membrane separation and adsorption techniques. Membrane separation has high separation efficiency, low energy consumption, and easy operation as an advantage but have a downside of requiring special equipment, membrane fouling, and high investment cost (Yaseen & Scholz, 2019). As a result, the only and straightforward method, adsorption as a high-quality treatment process by using adsorbent is the most preferable and desirable method for the removal of MB dye. The process of adsorption has an edge over the other methods due to its low regeneration cost, simplicity of design and operation, less land area requirement, not affected by toxic chemicals, and does not form harmful substances. Different adsorbents have been used to remove methylene blue from wastewater. But those adsorbents which have high removal capacity, low cost, and easy accessibility are no question of being a choice for industrial wastewater treatment process. Therefore, it is urgent need to develop cost effective and efficient dye removing technology, by increasing research attention using alternative low cost adsorbent. Thus, this investigation was performed by understanding the above interest and aimed to achieve effective and efficient method to the synthesis of magnetite (Fe_3O_4) iron oxide nanoparticle by chemical and biological (leaf extracts of *Prosopis julifera*) for removal of methylene blue dye.

1.3. Objectives

1.3.1. General Objective

The main objective of this research is to synthesize magnetite iron oxide (Fe_3O_4) nanoparticles by chemical and green (*Prosopis julifera* leaf extract) method and its applications for removal of methylene blue from aqueous solution.

1.3.2. Specific Objectives

The specific objectives of this sstudy are:

- To synthesize Fe_3O_4 nanoparticles using extract of *Prosopis julifera* leaf and iron salt precursors (through green) and chemical (co-precipitation) methods.
- To characterize the synthesized nanoparticles using different analytical methods (such as; XRD, SEM-EDX, FT-IR, UV-visible).
- To investigate the effect of pH, adsorbent dosage, contact time, and initial concentration in removal efficiency of methylene blue from aqueous solution.
- To evaluate the adsorption process of the synthesized Fe_3O_4 nanoparticle through adsorption isotherm and adsorption kinetics.

1.4. Significance of the Study

In the environmental remediation process, removal of different pollutants such as the separating of heavy metals and dyes like methylene blue from aqueous solution, iron oxide nano particles are preferable because they can react longer, disperse better, and reach locations farther than bigger particles. This study highlights the significance of chemical and green synthesis approaches and the role of biocompatible Fe_3O_4 nanoparticles in technological and economically feasible processes and green method practices of *Prosopis julifera*. It also summarizes the question of the sustainable synthesis process of Fe_3O_4 NPs using P. *julifera* for their application to the field of removal of methylene blue from aqueous solution. From the outcome of these studies, new coming researchers are benefited. It motivates industrial researchers to know the role of P. *julifera a* plant leaf extract in the green synthesis of magnetite (Fe_3O_4) nanoparticles for removal of methylene blue from aqueous samples and opens up the door for further research

on the use of P. *julifera* in the area. This study gives information for the researchers about synthesis and helps to use Fe_3O_4 nanoparticles (NPs) that are synthesized by biological (green method) and chemical methods for removal of methylene blue from aqueous solution in a low-cost, simple and environmental eco-friendly industrial researchers and comparing its removal efficiency of this dye by magnetite that synthesized through both chemical and green method.

1.5. Scope of the Study

The synthesis technique takes place by the chemical (co-precipitation) techniques and biosynthesis techniques were used for synthesizing Fe_3O_4 nanoparticles and characterized analytical methods such as UV-Visible spectroscopy (UV-Visible), Fourier transform infrared Spectroscopy (FT-IR), X-ray diffraction (XRD), Scanning electron microscopy (SEM) technique and its application for removal of methylene blue aqueous samples.

CHAPTER TWO

2. LITERATURE REVIEW

2.1. Nanomaterials for Wastewater Treatment

Nanomaterials are normally customary materials with enhanced properties and recently developed high-performance materials. Moreover, they may be of all material types (e.g., metals, polymers, ceramics), and they are inclusive of semiconductors, nanoengineered materials, and biomaterials. The majority of old-style techniques like adsorption, extraction, and chemical oxidation are, in general, effectual for wastewater treatment but are extremely costly. In that sense, advanced nanomaterials may play a leading role (Krishnaraj et al., 2012).

Nanoparticles show unique size-dependent physical and chemical properties, for example, optical, magnetic, catalytic, thermodynamic, and electrochemical. Organic and inorganic nanoparticles are materials of two or more dimensions, with a size in the range of 1–100 nm. Nanoparticles show unique size-dependent physical and chemical properties, for example, optical, magnetic, catalytic, thermodynamic, and electrochemical. Different types of nanomaterials like those that are nano adsorbents, nano-composite, and metal nanoparticles with active surface areas. Metal nanoparticles are investigated to overcome significant heavy metals like lead, arsenic, cadmium, mercury, copper, chromium, nickel, and dyes like methylene blue. They have shown a great ability to overcome activated carbon (Chiriac et al., 2016). Metal nanoparticles can be produced by comparatively low-budget preparation methods. Having high adsorption capacity, lower cost, easy separation and regeneration gives them an advantage from a technological and economical point of view. On the other hand, metal oxide nanoparticles like iron oxide are efficient uncostly adsorbents for various dye removal. Their adsorption capacity is primarily contingent on the interaction between adsorbate ions and the oxygen in metal oxides (Aba-Guevara et al., 2017). These nanoparticles could be directly applied as adsorbents or as core-shell materials where the shell proposes the desirable role and the core magnetically separates the contaminant.

In the past decade, the synthesis of magnetic iron oxide nanoparticles (IONPs) has been intensively developed not only for its fundamental scientific interest but also for its many

technological applications, such as targeted drug delivery, magnetic resonance imaging (MRI), magnetic hyperthermia and thermal ablation, bioseparation, and biosensing (Yang. 2008, Lee and Hyeon. 2012, Laurent et al., 2011, Cao et al., 2012). Particularly, bioapplications based on magnetic nanoparticles (NPs) have received considerable attention because NPs offer unique advantages over other materials. For example, magnetic IONPs are inexpensive to produce, physically and chemically stable, biocompatible, and environmentally safe (Lua. 2007). Eight iron oxides are known, among these iron oxides, hematite (α-Fe_2O_3), magnetite (Fe_3O_4), and maghemite (γ-Fe_2O_3) are very promising and popular candidates due to their polymorphism involving temperature-induced phase transition. Each of these three iron oxides has unique biochemical, magnetic, catalytic, and other properties which provide suitability for specific technical and biomedical applications (Cornell and Schwertmann. 2003).

Hematite (α-Fe_2O_3) as the most stable iron oxide and n-type semiconductor under ambient conditions, and hematite (α- Fe_2O_3) is widely used in catalysts, pigments, and gas sensors due to its low cost and high corrosion resistance. It can also be used as a starting material for the synthesis of magnetite (Fe_3O_4) and maghemite (γ-Fe_2O_3), which have been intensively pursued for both fundamental scientific interests and technological applications in the last few decades (Wu et al., 2010). Hematite is an n-type semiconductor with a band gap of 2.3 eV, where the conduction band (CB) is composed of empty d-orbitals of Fe^{3+} and the valence band (VB) consists of occupied 3d crystal field orbitals of Fe^{3+} with some admixture from the O 2p non-bonding orbitals (Zhang et al., 1993). As shown in figure 1(a), Fe^{3+} ions occupy two-thirds of the octahedral sites that are confined by the nearly ideal hexagonal close-packed O lattice.

Maghemite (γ-Fe_2O_3) as shown in Figure 1(c), the structure of γ-Fe_2O_3 is cubic; each unit of maghemite contains 32 O^{2-} ions, 21⅓ Fe^{3+} ions, and 2⅓ vacancies. Oxygen anions give rise to a cubic close-packed array while ferric ions are distributed over tetrahedral sites (eight Fe ions per unit cell) and octahedral sites (the remaining Fe ions and vacancies). Therefore, the maghemite can be considered as fully oxidized magnetite, and it is an n-type semiconductor with a bandgap of 2.0 eV. Magnetite (Fe_3O_4) as shown in Figure 1(b), Fe_3O_4 has the face-centered cubic spinel structure, based on 32 O^{2-} ions and is close-packed along the direction. Fe_3O_4 differs from most other iron oxides in that it contains both divalent and trivalent iron. Fe_3O_4 has a cubic inverse spinel structure that consists of a cubic close-packed array of oxide ions, where all of the Fe^{2+}

ions occupy half of the octahedral sites and the Fe^{3+} are split evenly across the remaining octahedral sites and the tetrahedral sites. In stoichiometric magnetite Fe (II)/Fe (III) = 1/2, the divalent irons may be partly or fully replaced by other divalent ions (Co, Mn, Zn, etc.). Thus, Fe_3O_4 can be both an n- and p-type semiconductor. However, Fe_3O_4 has the lowest resistivity among iron oxides due to its small band gap (0.1 eV) (Boxall et al., 1996).

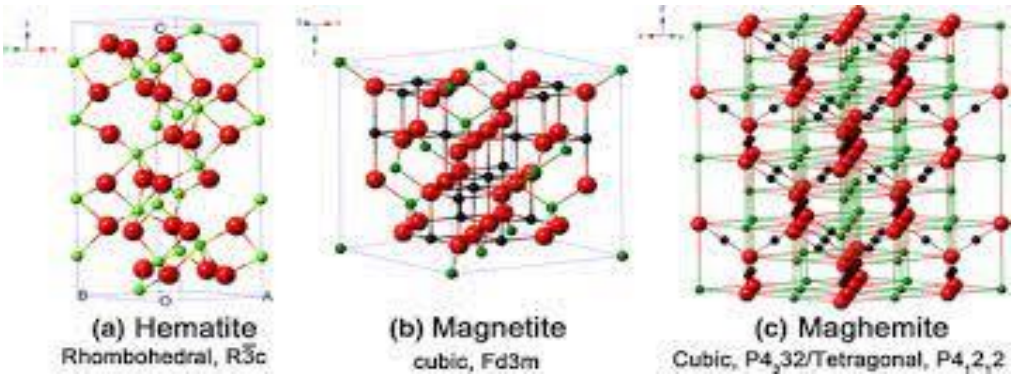

Figure 1: Crystal structure and crystallographic data of the hematite, magnetite, and maghemite (the black ball is Fe^{2+}, the green ball is Fe^{3+} and the red ball is O^{2-} (Jiang et al., 2015).

2.2. Magnetite (Fe_3O_4) Iron Oxide Nanoparticles

Recently, using magnetite (Fe_3O_4) iron oxide nanoparticles for heavy metals removal has drawn great interest owing to their availability and simplicity. Magnetic magnetite (Fe_3O_4) is frequently used as nano adsorbents. Mostly, due to the small size of nano adsorbent materials, their separation and recovery from the treated water are challenging issues. Thus, some researchers have excellently used these materials as sorbent materials for removing various heavy metals from wastewater systems (Ge et al, 2012). Adsorption efficiency increased and other metal ions interference decreased by functionalization of iron oxide nanoparticles (IONPs) by adding different ligands for controlling their adsorption features. They exhibit a hydrophilic surface due to the presence of hydroxyl groups. Because of its polymorphism, magnetite (Fe_3O_4) is one of the most interesting crystallographic phases of iron oxide, especially in its nanosized forms. It exhibits four different crystalline polymorphs with unique magnetic properties.

Fe_3O_4 nanoparticles have attracted intensive research interest because of their important applications in cancer therapy, drug delivery, magnetic resonance imaging (MRI), and

wastewater treatment (Vicky et al., 2010). For this application, certain parameters must be controlled during the synthesis. The control of the size, as well as size distribution, is necessary because it allows the control of the properties of the material such as superparamagnetism. Depending on their size, Fe_3O_4 nanoparticles present different behaviors when an external magnetic field is applied. It is known that abrupt changes in magnetic properties occur when the particle size is reduced from the micrometer to the nanometer scale.

2.2.1. Synthesis of Fe_3O_4 nanoparticle

The manufacture of nanoparticles can be broadly defined into two approaches. The first is the top-down approach and involves a material undergoing significant size reduction via physical processes (Birnbaum A. J. & Pique.A, 2011). During size reduction, the resulting particle size, shape, and surface structure are heavily dependent on the technique used. Unfortunately, size reduction also tends to introduce surface imperfections that can significantly impact the overall physicochemical properties of the fabricated nanoparticle. The second, bottom-up approach builds nanoparticles via the assembly of atoms, molecules, and smaller particles or monomers (Cheng et al., 2013). There are three main routes for the synthesis of Fe_3O_4: chemical, physical and biological methods. These have been investigated in order so produce more stable, soluble, biocompatible, and shape and size-controlled nanoparticles. (Jiang et al., 2008).

A. Physical method of Fe_3O_4 nanoparticles synthesis

The physical forces are used as an attraction of nano-scale particles for the formation of stable and well-defined nanoparticles. Examples are the plasma method, laser ablation, and thermal evaporation. In physical methods, nanoparticles are prepared by evaporation-condensation using a tube furnace at atmospheric pressure. The absence of solvent contamination in the prepared thin films**,** speed; radiation used as reducing agents, no involvement of hazardous chemicals, and the uniformity of NPs distribution are the advantages of physical synthesis methods in comparison with chemical processes. The disadvantages of physical methods, for example, tube furnace occupies a large space, consumes a great amount of energy while raising the environmental temperature around the source material, and requires a lot of time to achieve thermal stability (Abou El-Nour et al., 2010).

B. Chemical method of Fe_3O_4 nanoparticles synthesis

Chemical methods are well-known and widely accepted methods for bulk production of iron oxide (Fe_3O_4**)** nanoparticles. Chemical preparation methods are simple, tractable, and efficient, in which the size, composition, and even shape of the NPs can be managed. There are many chemical methods such as chemical co-precipitation, thermal decomposition, and sol-gel and hydrothermal methods for bulk production of iron oxide nanoparticles. However, in all these techniques, an aqueous medium is the most efficient pathway to obtain iron magnetic NPs. The size, shape, and composition of Fe_3O_4 NPs synthesized through chemical methods depend on the type of salt used, Fe^{2+} and Fe^{3+} ratio, pH, and ionic strength (Sun et al., 2011). Co-precipitation is the most universal method for producing iron oxide nanomaterials. For typical co-precipitation synthesis methods, the pH of a Fe (II) or Fe (III) ion solution is increased through the addition of a base. Chemical co-precipitation has been engaged as a cheap and suitable method for producing Fe_3O_4 nanoparticles to be used as magnetic drug carriers Fe_3O_4 can be synthesized through the co-precipitation of Fe^{2+} and Fe^{3+} by the addition of a base.

$$Fe^{+2} + 2Fe^{+3} + 8OH^- \longrightarrow Fe_3O_4 + 4H_2O$$

C. Biological (green) method of Fe_3O_4 nanoparticles synthesis

An alternative way of synthesizing metallic nanoparticles is made by using living organisms and its approach has received major attention for the synthesis of Fe_3O_4 of oxide nanoparticles. Although a variety of chemical and physical methods of synthesis are known, green synthesis is safer, sustainable, and biologically acceptable. The bio-reduction synthesis involves the use of different biological entities, such as plant extracts, bacteria, fungi, and yeasts. Plants and microbes are the main biological materials used for green synthesis. Iron oxide nanoparticles (IONPs) produced by plants, fungi, bacteria, and algae usually fall in the 1–100 nm range and are of distinct shapes like cubic, tetragonal crystalline, spherical, cylindrical, etc. Plants are considered an ecological way for nanoparticle synthesis, especially for those materials which have to be used in the biomedical removal of contaminants from the waste water field (Mittal et al., 2013; Saba, 2015)**.** Plants are generally considered freely available, easy to handle, harmless, and cheap material for the synthesis of various types of nanoparticles (Rauwel et al, 2015). The

biosynthesis process utilized distinct parts like roots, leaves, seeds, flowers, fruits, peels, and petals as reagents. Current reports also speculate that nanoparticles that are synthesized by using plant extracts are much more stabilized than the conventionally synthesized nanoparticles and extensive research is carried out on the synthesis of IONP by plant extract. Phytochemicals present in plants are capable of reducing the metal ions in comparatively less time (Singh et al.,2018). *Prosopis julifera* leaf phytochemicals analysis contains different classes of natural constituents: flavonoids, alkaloids, saponins, crude fiber, ash content, Pectic Substances, phenols, and tannins (Muhammad et al., 2013), and these constituents are used for different antimicrobial and heavy metals excretion.

2.2.2. Properties of Fe_3O_4 nanoparticle

Due to their size (diameters ranging from 1 to 100 nm), nanoparticles present specific and controllable properties that are different from those they present on the macroscopic scale thus enabling unique applications (Yetter et al., 2009). It is known that the ratio between the number of surface atoms and the number of massive atoms increases significantly with particle size reduction. As the surface atoms have less coordination with massive atoms, nanostructured materials exhibit significantly different physical, chemical, optical, electrical, and also magnetic properties.

Chemical properties

Magnetite is amphoteric, i.e., it can behave as an acid or a base. The reactive sites at the surface are hydroxyl groups (OH) and the density of groups has been measured as 5 per square nanometer. Freshly ground natural magnetite has a pH of 6.5 (Milonjić et al. 1983). Chemically, Fe_3O_4 nanoparticles (NPs) are very active and can easily be oxidized in air, generally resulting in the loss of dispersibility and magnetism. Thus, it is important to keep the stability of magnetic Fe_3O_4 NPs by developing some effective protection strategies and providing proper surface coating (or grafting) with organic molecules, polymers, surfactants, biomolecules, or inorganic layers such as silica, metal, metal sulfide, metal oxide, or nonmetal elementary substances (Wu et al., 2009). The respective synthesis method of Fe_3O_4 can affect their size and crystal structure (Estelrich et al., 2015).

Physical properties

It is chemically inert but is dissolved slowly by acids or bases at high temperatures (Ziemniak etal.1995). The dissolution rate depends on the surface area, pH, complexing ligands, presence of oxygen, and dissolved salts such as Fe^{2+}, UV light, and temperature**.** Natural and synthesized magnetite micro-scale crystals exhibit metallic luster and opaque jet black color, as shown in Table 1.

Table 1: Physical properties of magnetite (Fe_3O_4) nanoparticle (Hemingway et al., 1990).

Color	Black, gray with a brownish tint
Enthalpy	-1115.7 kJ/mol
Entropy	146.1 kJ/mol/K
Specific gravity	5.17–5.18
Crystal system	Isometric
Diagnostic properties	Dissolves slowly in hydrochloric acid
Hardness	5.5–6.5
Density	5.18 g/cm^3

Electrical properties

Magnetite has significant electrical conductivity and is considered a half metal (Chang et al. 2007). It is a semiconductor and has a small band gap of just 0.1 e V due to electron exchange between Fe^{2+} and Fe^{3+}. The electrons coordinated with these iron species are thermally delocalized and migrate within the magnetite structure causing high conductivity exchange constants: ranging from -28 J·K to 3 J·K between tetrahedral/octahedral sites and octahedral/octahedral sites, respectively. Due to electron delocalization effects magnetite can be slightly metal deficient on octahedral sites; such deficiency allows for n- and p-type magnetite semiconductors (Cornell &Schwertmann, 1996).

Magnetic properties

It is often assumed that magnetite is “magnetic,” i.e., it acts as a magnet and will attract ferrous metals or neighboring magnetite particles. Magnetite is ferromagnetic, meaning that it is

attracted to a magnet but is not itself magnetic. It is the most magnetic (i.e., strength of attraction to a magnet) of all the naturally occurring minerals (Harrisonetal.2002) with a saturation magnetization of 480 G at room temperature (Pullaiahetal.1975). The magnetic properties of a material depend on temperature, the applied magnetic field, and pressure. A change in these variables will result in the existence of two or more forms of magnetism. Ferro- and ferromagnetic materials like Fe_3O_4 and some of their alloys have particles whose shape is asymmetrical when they are obtained by the grinding of bulk materials. The magnetic Fe_3O_4 adsorbent particles adsorb the metal ions and sequentially accumulated; thus, the wastewater is treated.

2.2.3. Application of Fe_3O_4 Nanoparticles

Magnetite is a remarkable material with unusual properties and diverse applications. Probably the best-known example is magnetite iron ore used for steel production, which consumes millions of tons per year in water purification, where very-high-purity magnetite is used as a feedstock to produce iron-based chemicals. There are many other less well-known places where we encounter magnetite. For example, true gun bluing is a thin layer of magnetite that passivates the surface of iron to help prevent corrosion and lend a decorative effect. Magnetite is widely used as pigments which, being inorganic, are highly weather resistant with enhanced properties and recently developed high-performance materials. In the present application of magnetite nanomaterials for the removal of heavy metals, metalloids, and organic pollutants (methylene blue) from water, mainly copper, lead, chromium, mercury, and arsenic due to their magnetic, physical, chemical, thermal, and mechanical properties, and conjunction with control of size, composition and morphology of growth, the synthesis of mono nanoparticle (MNP) lead to a wide range of specific technological applications (Teja and Koh., 2009).

I. Fe_3O_4 nanoparticles as nano sorbent for heavy metals

Heavy metal contamination is of great concern because of its toxic effect on plants, animals, and human beings, and its tendency for bioaccumulation even at relatively low concentrations. Nowadays, the majority of bench-scale research and field applications of materials for wastewater treatment have focused on magnetic nanomaterials (NMs). Magnetic nano adsorbents

are strong adsorbents for the removal of pollutants from wastewater. The application of magnetic separation on the nano adsorbents provides the invaluable benefit of the rapid recovery of toxic metals and organic pollutants from wastewater (Singh, R et al., 2020). Among them, Magnetite nanoparticles are a promising solution because they are hydrophilic, super paramagnetic, and have a high surface area (Bagbi, Y et al., 2017). Iron oxide magnetic nanoparticles, possessing the capability to treat large volumes of wastewater and being convenient for magnetic separation, are the most promising materials for heavy metal treatment. The small size of Fe_3O_4 nano adsorbents is favorable for the diffusion of metal ions from the solution onto the active sites of the surface of the adsorbent. It recommended that Fe_3O_4 nano adsorbents were effective and economical adsorbents for rapid removal and recovery of metal ions from wastewater effluents. The efficient implementation of magnetic nano adsorbents depends on their efficiency in the selective adsorption of the pollutants involved and their surface chemistry.

II. Fe_3O_4 nanoparticles as nano sorbent for organic contaminants

Iron oxide nanomaterials (IONMs) are currently being explored for organic contaminant adsorption, particularly for the efficient treatment of large-volume water samples and fast separation via employing a strong external magnetic field. A lot of experiments have been undertaken to examine the removal efficiency of organic pollutants by using iron oxide nanomaterials (NMs) for organic pollutants (Zhang et al., 2010). For example, Fe_3O_4 hollow nanospheres were shown to be an effective sorbent for red dye (with a maximum adsorption capacity of 90 mg g^{-1}) (Iram et al., 2010). These proved that magnetic NMs technology was a novel, promising and desirable alternative for organic contaminant adsorption. Methylene blue ($C_{16}H_{18}N_3SCl$) is considered a typical heterocyclic aromatic compound, and it is used in many areas of biology and chemistry. It generally is an odorless, dark-green powder and forms a blue-colored solution when dissolved in an aqueous medium. In 1887, Paul Ehrlich reported that its exposure can cause supravital or intravital impacts, damaging nerve fibers (Krafts et al., 2012). Recently, synthesized super magnetic Fe_3O_4 nanoparticles and coated them with green tea poly-phenols (GTP) for dye removal from an aqueous solution.

2.3. Dyes

Dyes are ionic, aromatic organic compounds with structures including an aryl ring with delocalized electron systems and also give color to the material. Mauveine, the first synthetic dye, was discovered in 1856 by William Henry Perkin (Khamparia, S., & Jaspal, D. K. (2017). Since then, thousands of new synthetic dyes have been produced. Unlike most organic compounds, dyes possess color because they absorb light in the visible spectrum (400–700 nm), have at least one chromophore (color bearing group), have a conjugated system, i.e. a structure with alternating double and single bonds, and exhibit resonance of electrons, which is a stabilizing force in organic compounds. When any one of these features is lacking from the molecular structure the color is lost. In addition to chromophores, most dyes also contain groups known as auxochromes (color helpers), such as carboxylic acid, sulfonic acid, and amino and hydroxyl groups. While these are not responsible for color, their presence can shift the color of a colorant and they are most often used to influence dye solubility. The largest consumer of these dyes is the textile industry accounting for around two-thirds of its market. It is estimated that 1015% of the dye is lost during the dyeing process and released with the effluent (Yunusa, U., & Ibrahim, M. (2019).

Dyes are usually classified based on their particle charge upon dissolution in an aqueous application medium such as cationic (all basic dyes), anionic (direct, acid, and reactive dyes), and non-ionic (dispersed dyes) (Yagub, M. T., Sen, T. K., Afroze, S., & Ang, H. M. (2014).
Anionic dyes are highly water soluble and difficult to remove by conventional methods. Nonionic dyes, also known as disperse dyes, do not ionize in an aqueous solution and their fused aromatic ring structure makes them highly resistant to degradation. However, a few cationic dyes like methyl blue can be easily removed by adsorption and advanced oxidation processes (Ahmad et al., 2015).
There are many harmful effects of dyes on the ecosystem such as:

- ✓ They pose acute as well as chronic effects on most of the exposed organisms.
- ✓ They can absorb or reflect sunlight which enters the water bodies and thus affect the growth of bacteria and cause an imbalance in their biological activities.

- ✓ They have complex molecular structures which makes them difficult to treat with common municipal treatment operations.
- ✓ Consume dissolved oxygen and affect the aquatic ecosystem

2.3.1. Methylene Blue dye

Methylene Blue (MB) is a heterocyclic aromatic chemical compound with the molecular formula, $C_{16}H_{18}N_3SCl$, Figure 2, and chemical name [3, 7-bis (Dimethylamino)-phenazathionium chloride Tetramethylthionine chloride]. MB is a basic aniline dye that forms a deep blue color in the oxidized state while it is colorless in its reduced form (leucomethylene blue). It is prepared by oxidizing dimethyl-phenylen diamine with ferric chloride in the presence of hydrogen sulfide (Sartape et al., 2017). It is utilized in coloring paper, dyeing cotton and wool, and coloring paper stocks. It dissociates in an aqueous solution in the same way that electrolytes dissociate into methylene blue cation and the chloride ion. The removal of methylene blue from any wastewater is most important due to the serious environmental damage that can occur as a result of contact with it, particularly in the case of human beings (Mulana, F., Djuned, F. M., Fadli, M., & Meilian, M. (2020).

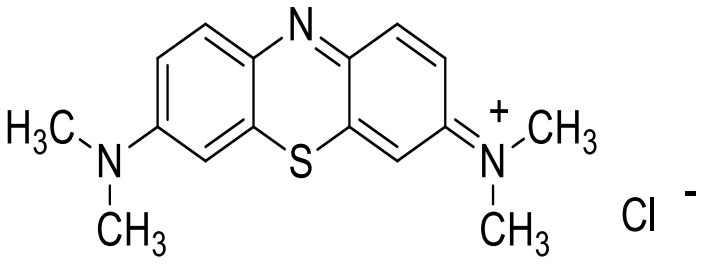

Figure 2: Molecular structure of Methylene blue (Sartape et al., 2017).

2.3.1.1. Properties of methylene blue dye

Some physical properties of methylene blue in Table 2 below.

Table 2: Physical properties of methylene blue

Properties	Values	Properties	Values
Structure of methylene blue	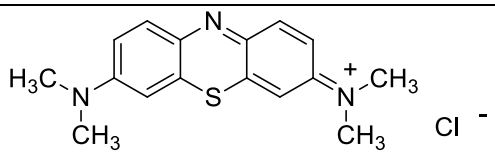	3, 7-Bis (dimethylamino) phenothiazin-5-ium	
Chemical name	Methylene Blue	Appearance	Dark green
Colour index	52015	Type	Basic Blue
Molecular formula	$C_{16}H_{18}ClN_3.3H_2O$	Physical state	Solid powder
Molecular weight	373.89	Bulk density(kg/m^3)	400-600
Maximum wave length(nm)	660	Water solubility(g/L) at 20 ℃	40

2.4. Dye removal technologies

With the growing rate of industrialization, the emission of effluents from different industries poses serious threats to several living forms due to their adverse effects. The serious environmental impact and increase in public awareness of environmental protection created a need to remove pollutants from wastewater before it is discharged into the environment. Currently, several methods can be used in the removal of dyes from industrial effluents. However, due to the variety of existent dyes and the effluent's complexity, not all methods have the same efficiency, and each method has its limitations. Generally, the treatment methods can be divided into three main categories namely physical, chemical and biological methods (Yuan et al., 2019).

2.5. Adsorption

Adsorption is a surface phenomenon in which adsorbate molecules or ions (liquid or gas) are concentrated on the surface of a solid. It is a process of binding molecules or particles onto the external surface of a solid or internal surface if the material is porous in a very thin layer (Kandasamy, Vigneswaran, Hoang, & Chaudhary, 2009). The binding to the solid is usually weak and reversible. The substance that accumulates at the interface is called 'adsorbate' and the solid on which adsorption occurs is known as 'adsorbent'. Adsorption takes place primarily on the walls of the pores or at specific sites inside the particle. Separation occurs because of differences in molecular weight, shape, or polarity, causing some molecules to be held more strongly on the surface than others. In many cases, the adsorbate is held strongly enough to allow complete removal of that component from the fluid. In the adsorption process, dye molecules may be adsorbed on the surface of an adsorbent through several forces such as hydrogen bonding, electrostatic interactions, van der Waals forces, hydrophobic interactions, etc. Generally, the adsorption process is classified as physisorption and chemisorption (Kandasamy et al., 2009).

Physisorption is a type of adsorption in which the forces of attraction are intermolecular forces (van der Waals forces) of the same kind as those responsible for the imperfection of real gases and the condensation of vapors, and do not involve a significant change in the electronic orbital patterns of the species involved. The adsorbed molecules are not fixed to a specific site at the surface of the adsorbent but are free to undergo translational movement within the interface. It is predominant at low temperatures and is characterized by relatively low energy of adsorption. Chemisorption is adsorption in which the forces involved are forces of the same kind as those operating in the formation of chemical compounds. Generally, adsorbents possess porous structures to increase the total exposed surface area and allow fluid to pass through faster (Samsami et al., 2020). The adsorption process is an attractive and effective alternative treatment for dye removal from wastewater (Sun, Zhang, Wang, & Wu, 2013).

There are many advantages of the adsorption process, such as:

- Less land area (half or a quarter of what is required in a biological system)
- Lower sensitivity to diurnal variation

- Toxic chemicals do not affect the process
- Greater flexibility in the design and operation
- Superior removal of organic contaminants
- The high dye removal efficiency
- The dose does not form harmful substances and is Easy to operation

2.5.1. Factors affecting the adsorption process

The initial dye concentration, solution pH, temperature, contact time, and adsorbent dosage are usually the main factors that govern the performance of most of the adsorption process. Optimization of such conditions greatly helps in the development of the industrial-scale dye removal treatment process. Some of the factors affecting the adsorption of dyes are discussed below.

Effect of solution pH

One important factor affecting the capacity of adsorbent in dye removal is solution pH. The efficiency of adsorption is dependent on the solution pH since variation in pH leads to the variation in the degree of ionization of the adsorptive molecule and the surface properties of the adsorbent (Yagub et al., 2014). The pH value of the solution determines the surface charge of the adsorbent which affects the interaction between the adsorbate and adsorbent. There are two possible mechanisms for the effect of pH on the adsorption of dyes on any adsorbent: electrostatic interaction between the protonated or deprotonated groups of adsorbents with dyes, and the chemical reaction between the adsorbate and the adsorbent. The hydrogen ion and hydroxyl ions are adsorbed quite strongly, and therefore, the adsorption of other ions is affected by the pH of the solution. The change of pH affects the adsorptive process through the dissociation of functional groups on the active sites of the adsorbent. This subsequently leads to a shift in reaction kinetics and equilibrium characteristics of the adsorption process. It is a common observation that the surface adsorbs anions favorably at lower pH due to the presence of H^+ ions, whereas, the surface is active for the adsorption of cations at higher pH due to the deposition of OH^- ions (Yagub et al., 2014).

Effect of adsorbent dose

Adsorbent dosage is an important process parameter to determine the capacity of an adsorbent for a given amount of the adsorbent at the operating conditions. Generally, removal efficiency increases with increasing adsorbent dosage, where the number of sorption sites at the surface of the adsorbent will increase by increasing the amount of the adsorbent. The effect of adsorbent dosage gives an idea of the ability of dye sorption to be adsorbed with the smallest amount of adsorbent, to recognize the capability of the adsorbent from an economical point of view (Sartape et al., 2017).

Effect of contact time

The contact time between the pollutant and the adsorbent is a significant importance in wastewater treatment by adsorption. The rapid uptake of pollutants and establishment of equilibrium in a short period signifies the efficiency of that adsorbent for its use in wastewater treatment. In physical adsorption, most of the adsorbate species are adsorbed within a short interval of contact time. However, strong chemical binding of the adsorbate with adsorbent requires a longer contact time for the attainment of equilibrium. Available adsorption studies in the literature reveal that the uptake of adsorbate species is fast at the initial stages of the contact period, and thereafter, it becomes slower near the equilibrium. In between these two stages of the uptake, the rate of adsorption is found to be nearly constant. This is obvious from the fact that a large number of vacant surface sites are available for adsorption during the initial stage, and after a lapse of time, the remaining vacant surface sites are difficult to be occupied due to repulsive forces between the solute molecules on the solid and bulk phases (Nasr, Hamdi, & Elhalouani, 2017).

Effect of dye concentration

The amount of adsorption for dye removal is highly dependent on the initial dye concentration. The effect of initial dye concentration depends on the immediate relation between the concentration of the dye and the available sites on an adsorbent surface. In general, the percentage of dye removal decreases with an increase in the initial dye concentration, which may be due to the saturation of adsorption sites on the adsorbent surface. On the other hand, the

increase in initial dye concentration will cause an increase in the capacity of the adsorbent and this may be due to the high driving force for mass transfer at a high initial dye concentration (Yagub et al., 2014).

2.6. Adsorption isotherm models

The equilibrium study on adsorption provides information on the capacity of the adsorbent. An adsorption isotherm is characterized by certain constant values, which express the surface properties and affinity of the adsorbent and can also be used to compare the adsorptive capacities of the adsorbent for different pollutants. It is the relationship that shows the distribution of adsorbate between the adsorbed phase and the solution phase at equilibrium (Yunusa & Ibrahim, 2019). If the adsorbent and adsorbate are contacted long enough, equilibrium will be established between the amount of adsorbate adsorbed and the amount of adsorbate in the solution. The equilibrium relationship is described by adsorption isotherms. Equilibrium data can be analyzed using commonly known adsorption systems. Several mathematical models can be used to describe experimental data of adsorption isotherms. The most commonly used isotherms are the Langmuir and Freundlich isotherms.

2.6.1. Langmuir isotherm model

Langmuir adsorption isotherm is one of the most popular isotherms for the removal of heavy metals, dyes, and organic pollutants by adsorption onto activated carbon, clay, agricultural waste, industrial waste, etc. It is valid for monolayer adsorption on specific homogenous sites containing a finite number of identical sites (Yunusa & Ibrahim, 2019). The basic assumptions underlying Langmuir's model which is also called the ideal localized monolayer model are that the molecules are adsorbed on definite sites on the surface of the adsorbent and each site can accommodate only one molecule (monolayer). The area of the site is fixed, the quantity is determined solely by the geometry of the surface, and the adsorption energy is the same at all sites. In addition, the adsorbed molecules cannot migrate across the surface or interact with neighboring molecules. The Langmuir isotherm model estimates the maximum adsorption capacity produced from the complete monolayer coverage on the adsorbent surface. Based upon

the above assumptions, the Langmuir isotherm model equation can be represented by equation 2.1 (Ramachandran, Vairamuthu, & Ponnusamy, 2011).

Langmuir:

$$q_e = q_m K_L C_e / 1 + K_L C_e \quad \text{.....2.1}$$

adsorption parameters were determined by transforming the above equation into a linear form.

$$1/q_e = 1/q_m + 1/q_m K_L C_e \quad \text{.....2.2}$$

Where:

q_e = amount of dye adsorbed per gram of the adsorbent at equilibrium (mg/g).

q_m = maximum monolayer coverage capacity (mg/g)

C_e = equilibrium concentration of adsorbate (mg/L)

k_L = Langmuir isotherm constant (L/mg)

The values qm and k_L can be computed from the slope and intercept of the Langmuir plot of 1/qe versus $1/C_e$. The essential features of the Langmuir isotherm may be expressed in terms of equilibrium parameter R_L, which is a dimensionless constant referred to as the separation factor or equilibrium parameter (Y. Zhang et al., 2019).

$$R_L = 1/1 + (1 + K_L C_o) \quad \text{..... 2.3}$$

Where:

R_L= Langmuir equilibrium parameter

C_0 = initial concentration (mg/L)

k_L = constant related to the energy of adsorption, Langmuir Constant (L/mg)

R_L value indicates the adsorption nature to be either unfavorable if $R_L > 1$, linear if $R_L = 1$, favorable if $0 < R_L < 1$, and irreversible if $R_L = 0$.

2.6.2. Freundlich isotherm model

Freundlich isotherm model assumes that the adsorption occurs on a heterogeneous surface and non-uniform distribution of the heat of adsorption over the adsorbent surface takes place (Yunusa & Ibrahim, 2019). Freundlich equation suggests multilayer adsorption and the sorption energy exponentially decreased on completion of the sorption centers of an adsorbent. It is assumed that the stronger binding sites are initially occupied with the binding strength decreasing with an increasing degree of site occupation (Sun et al., 2013).

The linearized form of Freundlich model is expressed as follows:

$$\text{Log } q_e = \log k_f + 1/\,n \log C_e \qquad \text{2.4}$$

Where:

q_e = amount of dye adsorbed per gram of the adsorbent at equilibrium (mg/g)

C_e = equilibrium concentration of adsorbate (mg/L)

k_f = Freundlich isotherm constant (mg/g)

n = adsorption intensity

The equilibrium adsorption capacity, qe (mg/g) can be calculated using the mass balance equation given.

$$q_e = V\frac{(Co-Ce)}{W} \qquad \text{2.5.}$$

Where C_o and C_e are the initial and final equilibrium concentration of adsorbate (mg/L), V is the volume of the solution (L) and W is the dry adsorbent (g). The amount of adsorbate adsorbed, qt (mg/g) at any time can be calculated using the Equation below.

$$Q_t = V\frac{(Co-Ct)}{W} \qquad \text{2.6.}$$

Where, C_t is the concentration of adsorbate, (mg/L) at any time.

The percentage removal of adsorbate can be calculated using the following relationship (Abdulabbas et al., 2020).

$$\% \text{ Removal of MB} = \frac{(Co-Ce)}{Co} \times 100 \quad \text{.....2.7.}$$

Where C_o and C_e are the initial and final equilibrium concentration of adsorbate (mg/L). The applicability of two adsorption isotherms (Langmuir and Freundlich) can be compared by evaluating the multiple regression correlation coefficients, R^2. In regression, the R^2 coefficient of determination is a statistical measure of how well the regression line approximates the real data points. R^2 is a number between zero and one that would give some information about the best fit of a model. If the value of R^2 is close to zero suggests a poor model. If the value of R^2 is 1.0 indicates that the regression line perfectly fits the data. If the value of R^2 occurs outside the range 0 to 1, it is used to measure the agreement between observed and modeled values (Fu et al., 2018).

2.7. Adsorption kinetics models

The dynamics of the adsorption can be studied by the kinetics of adsorption in terms of the order of the rate constant. The adsorption rate is an important factor for a better choice of material to be used as an adsorbent; where the adsorbent should have a large adsorption capacity and a fast adsorption rate. Most adsorption studies used Pseudo-first-order and Pseudo-second-order models to study the adsorption kinetics (Kheddo et al., 2020).

2.7.1. Pseudo-first-order kinetics model

The pseudo-first-order kinetics model is one of the most widely used rate equations to describe the adsorption of adsorbate from the liquid phase. The linear form of the pseudo-first-order rate is given in equation 2.8 (Ramachandran et al., 2011).

$$\text{Log}\,(q_e - q_t) = \log q_e - k_1 t / 2.303 \quad \text{.....2.8.}$$

Where: q_e and q_t = adsorption capacity at equilibrium and at time t, respectively (mg/g)

k_1 = rate constant of pseudo-first-order kinetics (min-1)

The plot of log ($q_e - q_t$) versus t should give a linear relationship from which k_1 and qe can be determined from the slop and intercept of the plot, respectively.

2.7.2. Pseudo-second-order kinetics model

The adsorption kinetics was also described as pseudo-second-order kinetics using equation 2.9.

$$t/qt = 1/k_2qe^2 + (1/qe)t \quad \text{2.9}$$

Where: qe and qt = adsorption capacities at equilibrium and at time t, respectively (mg/g)

k_2 = rate constant of pseudo-second-order sorption (g/mg/min)

If Pseudo-second order kinetics is applicable, the plot of t/qt against t should give a linear relationship, from which qe and k_2 can be determined from the slope and intercept of the plot (Zhang et al., 2016).

2.8. *Prosopis julifera* Plant in Ethiopia

Prosopis julifera species is one of the most highly invasive plants in the world. *Prosopis julifera,* in its scientific name, and Ethiopia, it is called 'Weyane/Dergi-Hara' and 'Biscuit' bureau respectively. It is a woody shrub (3-5 m tall) or tree (up to 15 m tall); bark thick, rough, and grey-green becoming scaly with age; often multi-stemmed, especially following cutbacks (coppicing), with abundant large and very sharp thorns measuring up to 5 cm; deeply rooted, Leaves: Doubly-divided composed leaves (6-8 cm long), each 6-16 mm long and 1.5-3.2 mm wide, Flowers: Seeds: Brown, oval. In Africa alone, *Prosopis julifera* is believed to have invaded over 4 million hectares, threatening crop and rangeland production, desiccating water resources, and displacing native flora and fauna (Witt, 2010). The *Prosopis julifera* infestation or the large area covered by this plant in Metahara is shown in Figure 3.

Figure 3*: Prosopis julifera* infestation in Oromia regional state, Metahara.

The wood is excellent fuel, the timber hard, and comparable to the finest hard woods. The sweet nutritious pods are relished by all livestock and are made into different food and drinks. Cylindrical or slightly irregularly curved green pods which turn yellow upon ripening (10-20 cm long); containing 10-20 hard oval or elliptical seeds (2.5-7 mm long). It is an important species because of its high nitrogen fixing potential in very dry areas and drought seasons and also because it provides shelter and food to many species of animals on its nectar, pollen, leaves, and fruits (Almaraz-Abarca et al., 2007). The shrubs of *Prosopis julifera* are highly esteemed for windbreaks, soil binders, sand stabilizers, living fences, fuel wood, bee plants, and animal feed (Allen et al.,2009). *Prosopis julifera has* many Impacts: Negative effects include complete loss of pasture and rangelands for both domestic and wild ruminants (such as cattle, goats, camels, and giraffes), losses due to restricted access to water, and illness and death of livestock due to eating the pods and being injured by the sharp and out thorns.

2.8.1. Phytochemicals analysis of *Prosopis julifera* leaves

The air-dried leaves of P. *julifera* were analyzed for chemical composition. The results revealed the quantitative analysis of the following classes of natural constituents as shown in Table 3.

Table 3: Quantitative phytochemical analyses of *Prosopis julifera* (Muhammad Ibrahim et al., 2013)

Phytochemicals	**Concentration in %**
Flavonoids	16 ± 0.39
Alkaloids	3.6 ± 0.06
Saponins	2.2 ± 0.23
Phenols	0.66 ± 0.11
Tannins	0.33 ± 0.07
Crude fiber	17.5 ± 0.14
Ash Content	9.5 ± 0.08
Pectic Substances	4.9 ± 0.18

The very high flavonoid content (16%) of *Prosopis julifera* makes it a potential candidate bearing antioxidant and anticancer properties. Tannins and Phenols although found in low concentrations, (0.33 and 0.66% respectively) can synergize the antioxidant and anticancer potential of flavonoids. Phenols are reported to prevent platelets from clumping and have the ability to block specific enzymes that cause inflammation. These also act as immune enhancers, anti-clotting, and hormone modulators. The presence of alkaloids indicates the pharmacological importance of plants because alkaloids and their derivatives are used as basic medicinal agents due to their analgesic, antispasmodic and bactericidal activities. Leaves of *P. julifera* can also be used as low-cost, highly nutritive, and digestible forage after processing with molasses or other feeds (Heuze et al., 2011).

CHAPTER THREE

3. MATERIALS AND METHODS

3.1. Chemicals and Instruments

All the chemicals and reagents used for the preparation of Fe_3O_4 nanoparticles and adsorption were analytical grade purchased from local chemical markets.

3.1.1. Chemicals and Reagents

Chemicals used in the experimental part of this work were presented in Table 4.

Table 4: Chemicals used in experiments

No	Name	Chemical Formula
1	Sodium hydroxide	NaOH (Sigma aldria 99% purity)
2	Ethanol	C_2H_5OH (99.8% purity)
3	Ferric chloride hexahydrate	$FeCl_3.6H_2O$ (Sigma aldria 99% purity)
4	Ferrous chloride tetrahydrate	$FeCl_2.4H_2O$ (Sigma aldria 99% purity
5	Methylene blue	MB (96% purity)
6	Hydrochloride acid	HCl (Riedel dehaen, Germeny, 37% v/v HCl)
7	*Prosopis julifera* leaf extract	PJLE
8	Distilled water	DW

All chemicals mentioned in Table 4 and some additional materials were purchased from laboratory chemical suppliers, in Addis Ababa, Ethiopia.

3.1.2. Apparatus and Instruments

The apparatus and equipment that were used during this research work were UV-Vis (T80+- PG instrument), Diffuse reflectance spectroscopy (UV-Vis DRS Elico SL-150 spectrophotometer), XRD (Shimadzu, XRD-7000S South Korea), FTIR (FTIR Perkin Elmers spectrophotometer), SEM (Scanning Electron Microscopy), TGA (Thermogravimetric Analysis), electronic balance,

oven, beaker, test tube, magnetic stirrer, mechanical grinder, Whatman No.1, filter paper, measuring cylinder, pH-meter, spatula, Erlenmeyer flask, volumetric flask, the ceramic crucible, funnel, and pipettes, dropper, beaker, mortar and pestle, and magnetic bar.

3.2. Synthesis of Fe_3O_4 Nanoparticle by Chemical (Co-precipitation) Method

2M NaOH solution was added and mixed in 200 mL (100 mL of each) of 0.2M ferric chloride hexahydrate ($FeCl_3.6H_2O$) and 0.1M ferrous chloride tetrahydrate ($FeCl_2.4H_2O$) solution after the solution was stirred on a magnetic stirrer at speed of 700 rpm for about 2 hours at room temperature until pH was attained to 11. Then the stirred solution was kept overnight at room temperature. Discarded the solutions that were found at the top very carefully followed by centrifugation at 2500 rpm for 15 min, then precipitated black color of Fe_3O_4 nanoparticles (NPs) was washed with distilled water and ethanol at least three times and collected using a crucible ceramic dish and placed into a drying oven for 24 hours at 80 ℃. Here Figure 4 shows the process of synthesizing Fe_3O_4 by the chemical (coprecipitation) method.

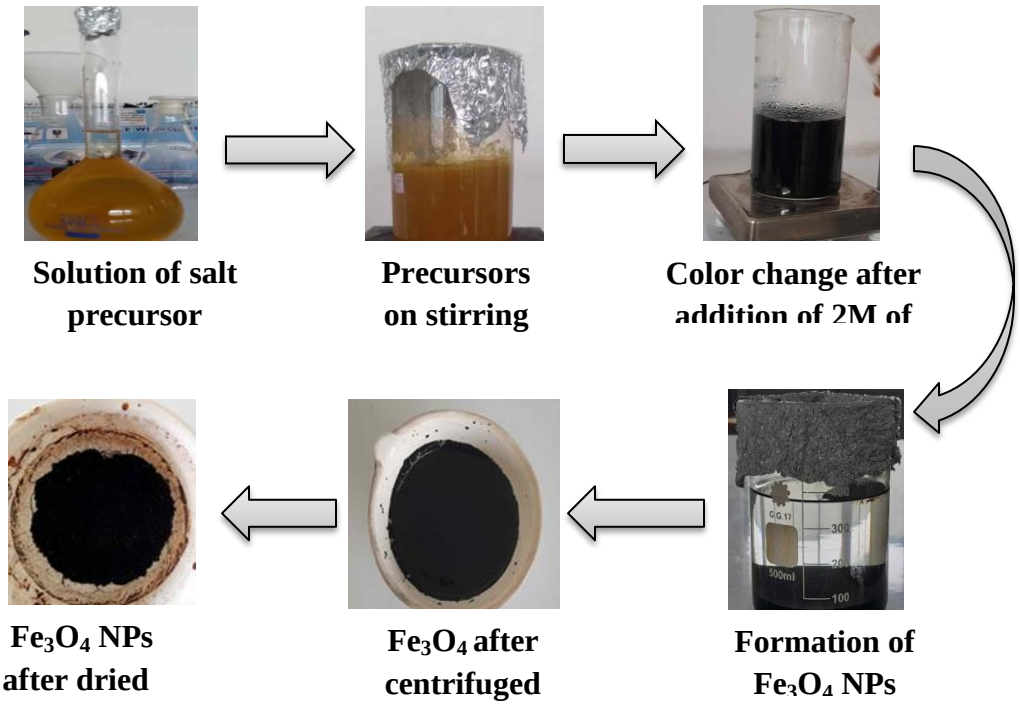

Figure 4: Schematic diagram of a synthesized process for Fe_3O_4 nanoparticles by chemical method.

3.4. Synthesis of Fe_3O_4 Nanoparticle by Green Method

3.4.1. Collection and preparation of plant material

Fresh plant leaves of *Prosopis julifera* were collected from Oromia regional state, Metahara town. Then, the collected leaf was washed for removing dust and any impurities by using distilled water and dried at room temperature. The dried leaf is cut and ground into powder. Then, the powder was sieved. The plant powder (20 g) was extracted by boiling with 500mL of distilled water in a volumetric flask at 50 ^{0}C for 1 hour. Then the resulting dark brown colored extract was cooled to room temperature and centrifuged. Finally, the extract was kept at 25 oC to be used for the synthesis of the target magnetic nanoparticles (Nurbas et al. 2017). Figure 5 shows the process for the preparation of *Prosopis julifera* leaf extract.

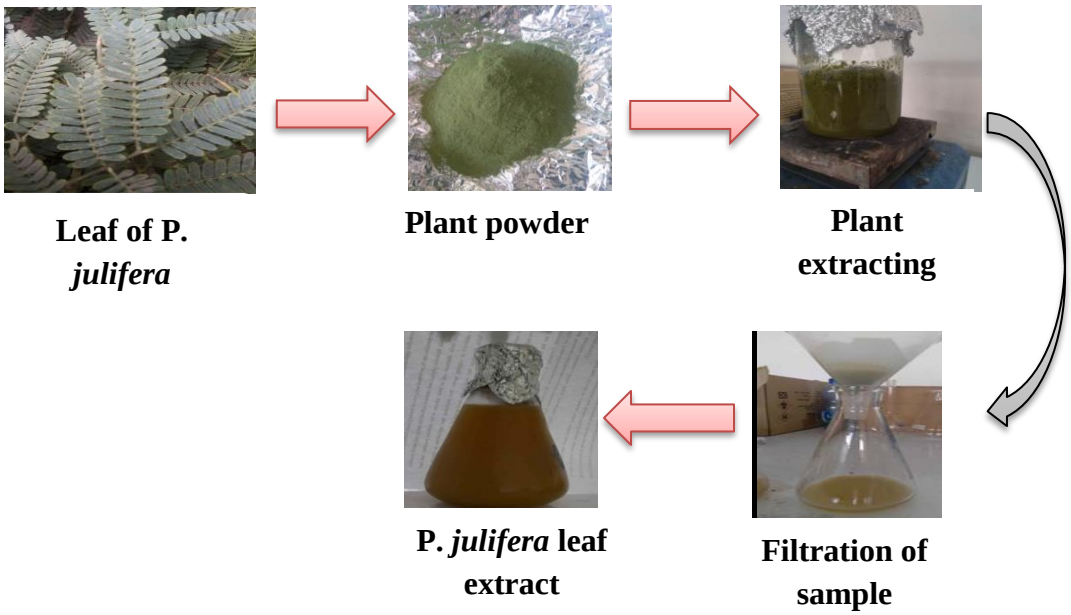

Figure 5: Preparation process of *Prosopis julifera* leaf extract.

3.4.2. Synthesis of Fe_3O_4 nanoparticles by using *Prosopis julifera* leaf extract

0.1 M $FeCl_2.4H_2O$ and 0.2 M $FeCl_3.6H_2O$ at 1:2 molar ratios were dissolved in distilled water by stirring at the speed of 700 rpm for 2 hours on a magnetic stirrer. Then, the same amount of leaf extract was added to the metal ions solutions. After the addition of the leaf extract, the color of the solution was changed to dark brown. The color change represents the formation of

nanoparticles. Then, 2.0 M of NaOH solution was added to the metal ion solution until the pH value was attained at11 (Nurbas et al. 2017). The specimen was then filtered to remove the solid product and washed with ethanol. Finally, the specimens were dried in an oven at 50 ℃ and prepared for characterization. In a typical experiment, the extract was added to ferric chloride and ferrous chloride precursors solution in three different ratios by volume. Figure 6 shows a process for synthesizing Fe_3O_4 nanoparticles by a green method.

For 1:1 ratio: 50mL of *Prosopis julifera* leaf extract and 50 mL (25 mL of each salt) of 0.2 M Ferric chloride heptahydrate, 0.1 M Ferrous chloride tetrahydrate.

For 1:2 ratio: 33.3mL of *Prosopis julifera* leaf extract and 66.6 mL (33.3 mL of each salt) of 0.2 M Ferric chloride heptahydrate, 0.1 M Ferrous chloride tetrahydrate.

For 2:1 ratio: 66.6mL of *Prosopis julifera* leaf extract and 33.3 mL (16.65 mL of each salt) 0.2 M Ferric chloride heptahydrate, 0.1 M Ferrous chloride tetrahydrate. The reaction principle is simply as:

$$Fe^{2+} + 2Fe^{3+} + 8OH^- \leftrightarrow Fe(OH)_2 + Fe(OH)_3 \rightarrow Fe_3O_4 + 4H_2O$$ (Guo et al., 2009).

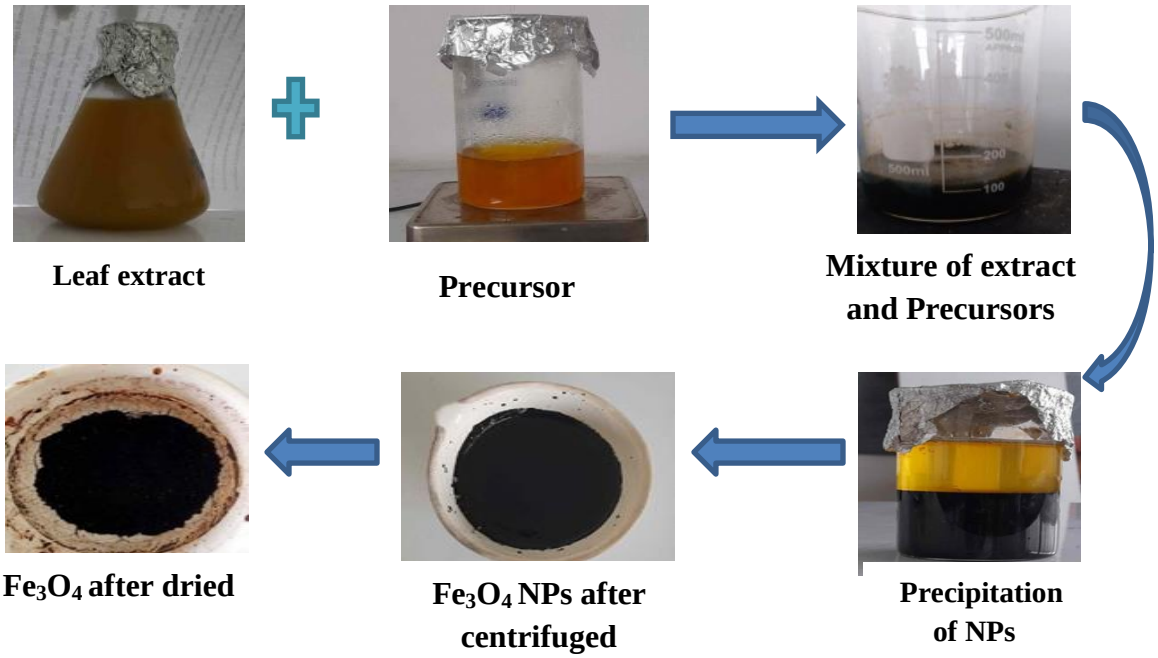

Figure 6: Schematic diagram of a synthesized process for Fe_3O_4 nanoparticles by a green method.

3.5. Characterization of the synthesized Fe_3O_4 Nanoparticle

The characterizations of the biosynthesized Fe_3O_4 nanoparticle were done by using TGA, FTIR, XRD, SEM, and UV-Vis Spectrophotometer.

3.5.1. Characterization of Fe_3O_4 Nanoparticles Using Thermo gravimetric analysis (TGA)

Thermal gravimetric analysis (TGA) was carried out using a simultaneous DTA-TGA apparatus (DTG-60H, Shimadzu Co., South Korea) to decide the calcination temperature and stability of the synthesized Fe_3O_4 nanoparticles. Thermogravimetric analysis of the biosynthesized Fe_3O_4 nanoparticles was done at Bahirdar University Chemistry Department in a flowing air atmosphere and the thermograms were recorded in the temperature range of 25–800 ^{0}C, at a heating rate of 20 ^{0}C/min.

Sample preparation: A piece specimen of powder (7 – 8 mg) was placed in a platinum basket and the temperature was continuously recorded by a thermocouple under the basket. While the sample was heated at a uniform rate in an appropriate environment, TGA measures the percent weight loss of a test sample.

3.5.2. Characterization of Fe_3O_4 Nanoparticles Using XRD

XRD was used to analyze the structure of the newly synthesized Fe_3O_4. The XRD was performed to investigate the crystalline or amorphous nature of magnetite nanoparticles. The main information obtained from XRD was crystal structure. The average particle size was calculated with Debye Scherer's formula.

$$D = \frac{0.94\lambda}{\beta c0s\theta} \quad \text{.....3.1.}$$

Where, D is the Crystallite size, (λ= 1.54 A^0 is the X-ray source wavelength, β is the Full Width at Half Maximum (FWHM) of a peak, and θ is the peak position (Arokiyaraj et al., 2013).

X-ray diffraction (XRD) analysis of the synthesized nanomaterial was done at Adama Science and Technology University, Material Engineering department. X-ray diffraction patterns of the

dried powder of the biosynthesized Fe_3O_4 NPs samples were recorded on Shimadzu XRD- 7000 X-ray diffractometer, copper emission as an X-ray source, with Ni filter, and wavelength of 1.5418 A^0. The samples were scanned in the 2θ range of 10–80 degrees, at a scanning rate of 3 deg/min.

Sample preparation: 1.5-2.5 grams of dried Fe_3O_4 NPs ground by mortar and paste and then it was filled into the sample holder and subjected to an X-ray diffractometer.

3.5.3. Characterization of Fe_3O_4 Nanoparticles Using FT-IR Spectroscopy

FTIR spectroscopic analysis was carried out to identify the functional groups and investigate the characteristic functional groups of iron oxides and the characterization of precursors from different synthesis methods. It was used to identify the possible biomolecules responsible for the reduction and capping of the nanoparticles after synthesis (Kumar and Ananthu, 2018). FTIR analysis of the synthesized nanomaterial was done at Bahirdar University Chemistry Department. FTIR spectrum of the dried powder of the chemically and biosynthesized Fe_3O_4 samples was recorded on 65 FT-IR (PerkinElmer) in the range 4000-400 cm^{-1}.

Sample preparation: The synthesized powders of the nanomaterial were mixed with potassium bromide (KBr) and diluted to form a very fine powder. The powder was then compressed into a thin transparent pellet which was used for recording FTIR spectrum.

3.5.4. Characterization of Fe_3O_4 Nanoparticles Using UV-Vis Spectroscopy

UV-Vis spectroscopy (spectrophotometry) is a quantitative technique used to measure how much a chemical substance absorbs light by measuring the intensity of light that passes through a sample to the intensity of light through a reference sample or blank. UV-Visible Spectrophotometer was used to determine the energy band gap of the synthesized adsorbent.

The UV-Vis absorption spectra of the Fe_3O_4 nanoparticles from *Prosopis julifera* leaf extract and that of chemically synthesized was confirmed by using wave length scan between 200 nm and 800 nm (Bhosale et al. 2014). From the UV-Vis graphs, the energy band gap was obtained using the formula:

$$Eg = \frac{hc}{\lambda} \quad \text{.....3.2}$$

Where; Eg is the energy band gap, h is planks constant, c is the speed of light and λ is the maximum wavelength of the synthesized Fe_3O_4 nanoparticles.

The optical properties and band gap energy of magnetite nanoparticles were characterized by UV-Vis spectrophotometers at Adama Science and Technology University Material Engineering Department. The range of absorption was between 250 nm to 950 nm.

Sample preparation: Finely ground powder of a standard ($BaSO_4$) and sample were carefully packed into a sample holder with a rectangular or circular hole with a surface of a few tens square millimeters to several square centimeters. Then the holder was placed horizontally at the bottom of the integrating sphere and absorbance spectra were recorded.

3.5.5. Characterization of Fe_3O_4 Nanoparticles Using SEM

Scanning electron microscope (SEM) is a type of versatile electron microscope that, due to its several characteristics, is commonly used to investigate the surface morphology (polished or rough) or subsurface sample with relatively large dimensions. SEM analysis of the biosynthesized Fe_3O_4 NPs was carried out at Adama Science and Technology University Biology Department which reveals information about the external morphology of the chemically and biosynthesized Fe_3O_4 sample with direct visualization.

Sample preparation: Small amount of powder sample was dispersed in acetone and sonicated for a few minutes. Some samples need to be coated to make them conductive. Metals require no preparation due to their inherent ability to conduct electricity. However, non-metals need to be coated with a conductive material such as gold/ gold-palladium alloy, using a sputter coater.

3.6. Methylene Blue (MB) Adsorption Study

3.6.1. Adsorption experiments

A batch adsorption experiment was performed by contacting a certain concentration of dye with the magnetite (Fe_3O_4) at specified process conditions. For this set of experiments, a 500 mg/L stock solution of methylene blue (MB) dye was first prepared and the needed concentration was

diluted from it in a 250 mL volumetric flask. The pH of the solution was adjusted by using 0.1 M HCl and 0.1 M NaOH to bring it to the required pH value. The appropriate concentration of the dye was mixed with the magnetite and put on an orbital shaker at 250 rpm at different times. The solution obtained after adsorption was centrifuged at 250 rpm for 10 min to separate the adsorbent from the supernatant. The supernatant is then measured for its remaining concentration using a UV-Vis spectrophotometer. The effects of various parameters such as dye initial concentration, contact time, pH, and adsorbent dosage were also studied. Finally, analysis of the concentration of methylene blue, the percentage removal of MB from the solution was calculated by equation 3.3.

$$\% \text{ Removal} = \frac{Co - Ct}{Co} * 100 \quad \text{.....3.3.}$$

Where C_0 (mg/L) is the initial MB concentration and C_t (mg/L) is the final MB concentration in the solution.

The adsorption capacity of MB was calculated by:

$$Q = \frac{(Ci - Cf)V}{M} \quad \text{..... 3.4.}$$

Where, Q- dye adsorption capacity (mg / g); C_i- concentration of dye (mg/L) in the solution before adsorption; C_f- dye concentration (mg/L) in the solution after adsorption; V- the volume of the solution (L); M- The amount of adsorbent (g).

3.6.2. Analysis of MB dye concentration using UV-Vis spectrophotometer

Calibration curve was needed to be set up to measure the concentration of MB dye in an aqueous solution using a UV-Vis spectrophotometer. The calibration curve is constructed by preparing orderly increasing concentration solutions and measuring the absorbance of this solution. MB absorbs UV-Vis light at a wavelength of 665 nm. An absorbance versus concentration linear graph was drawn and the equation of the straight line was determined. So samples from the absorption studies are brought and their absorbance measured. The concentration of the solutions was then determined from the calibration graph. Here Figure 7 show the linear calibration curve pot for methylene blue dye and Figure 8 show the UV-Vis light spectrum of MB dye.

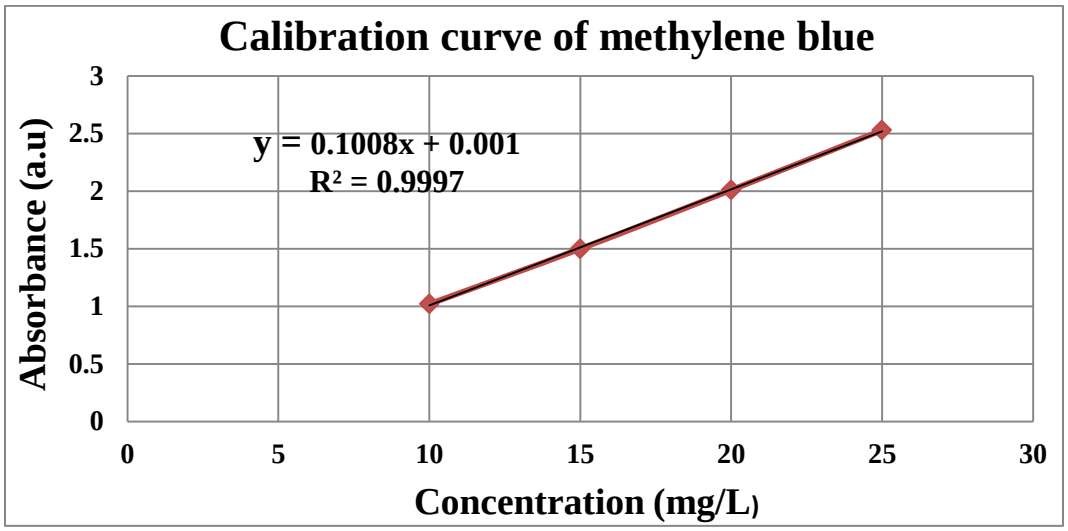

Figure 7: Calibration line for determination of methylene blue dye (absorbance in a.u (y) Vs concentration in mg/L (x)).

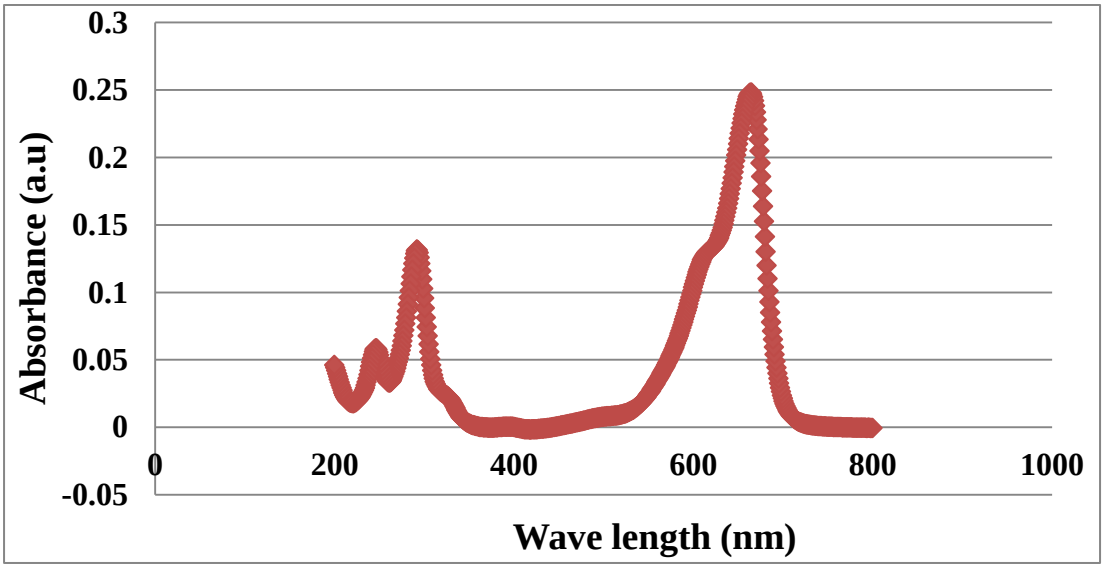

Figure 8: UV-Vis light spectrum of MB dye.

3.7. Adsorption Isotherms

When a solution is contacted with a solid adsorbent, molecules of adsorbate get transferred from the fluid to the solid until the concentration of adsorbate in the solution as well as in the solid phase are in equilibrium. At equilibrium, equal amounts of solute eventually are adsorbed and

desorbed simultaneously. This is called adsorption equilibrium. Sorption isotherm is an empirical relationship used to predict how much solute can be adsorbed by the adsorbent. Adsorption isotherm is defined as a graphical representation showing the relationship between the amount adsorbed by a unit weight of adsorbent and the amount of adsorbate remaining in a test medium at equilibrium, and it shows the distribution of an adsorbable solute between the liquid and solid phases at various equilibriums. The equilibrium data at a given temperature are represented by the adsorption isotherm. Adsorption isotherm models such as Langmuir and Freundlich models were used to fit the experimental data. It helps to find out the best fitting isotherm model to evaluate the efficiency of the prepared adsorbent and to develop a suitable batch absorber design.

3.8. Kinetic Studies of the adsorption process of MB by Fe_3O_4 nano particle

Adsorption kinetics is a curve (or line) that describes the rate of retention or release of a solute from an aqueous environment to a solid-phase interface at a given adsorbents dose, temperature, flow rate, and pH (George William Kajjumba, 2018). The adsorption kinetics of methylene blue was studied to determine the required exposure time to achieve equilibrium adsorption of methylene blue on the adsorbents. In this research, the kinetics was investigated experimentally under different values of initial concentration of methylene blue, pH, and magnetite nano particle dosage by using pseudo-first-order and pseudo-second reaction models.

3.9. Experimental design for adsorption of methylene blue by Magnetite (Fe_3O_4) nano particle

Among the many experimental operating parameters that may influence the adsorption process, the most important factors include the solution pH, adsorbent dose, contact time, and initial concentration. For finding optimum conditions of the parameters for metal removal efficiency of iron nano particle data analysis was performed. The experiment was designed to investigate the single effects of selected optimum parameters. All various values of the above parameters used during the adsorption process are listed in Table 5.

Table 5: Experimental design for the batch adsorption study

Parameters	Ranges and Levels				
	1	2	3	4	5
pH	3	5	7	9	11
Contact time (min)	20	40	60	80	100
Adsorbent dosage (g)	0.1	0.2	0.3	0.4	0.5
Initial concentration (mg/L)	10	20	30	40	50

3.10. Reusability Experiment

To study the regeneration and reusability of the adsorbent, batch adsorption experiments were conducted with a magnetite (adsorbent) dosage of 0.5 g and an initial dye concentration of 10mg/L at room temperature with a stirring rate of 150 rpm. The adsorbent was recovered after the experiment through centrifugation and filtration, followed by washing with 0.1M NaOH and distilled water and drying. The same procedure was repeated 5 times for both the green and chemical methods.

CHAPTER FOUR

4. RESULTS AND DISCUSSION

This section discussed the result of green (biological) synthesized and chemical synthesized iron oxide magnetite (Fe_3O_4) nanoparticles by using different precursors depending on their method of synthesized. In the green method iron oxide (Fe_3O_4) nanoparticles synthesis in three different ratios from ferrous chloride tetrahydrate and ferric chloride hexahydrate as precursors and leaf of P. *julifera* extract as a reducing and capping agent. In the chemical method iron oxide (Fe_3O_4) nanoparticles were synthesized from ferric chloride and ferrous chloride in 2:1 ratios. Also, the different characterization methods (TGA-DTA, XRD, FTIR, UV-Vis Spectroscopy, SEM) of green synthesis and chemically synthesized iron magnetite oxide magnetite nanoparticles and their application for removal of methylene blue from aqueous solution were presented.

4.1. Characterization of Iron Oxide (magnetite) Nanoparticle

4.1.1. Thermo Gravimetric Analysis (TGA) Result

Figure 9 shows the Thermo gravimetric analysis (TGA) and differential thermal analysis (DTA) of the uncalcined Fe_3O_4 NPs. TGA curve shows mass loss of the sample whereas the DTA curve indicates the energy gain or loss during the process. The first weight loss of about 4.94 % happened at 200 °C and an endothermic peak was detected at approximately 160.06°C, which was related to the evaporation of H_2O on the surface and precursor building, while the second weight loss reported being 6.65 % occurred in the temperature range of 210 ^{0}C - 366 ^{0}C is associated with the degradation of capping materials and organic compounds (Marluce Oliveira da Guarda Souza, 2020). Such processes are exothermic, as evidenced from the peaks in the DTA curve, at temperatures of 288.3 ^{0}C and 306 ^{0}C. In the temperature range up to 435 ^{0}C, 11.59 % of total weight loss was observed. No considerable loss was observed after 435 ^{0}C. This indicates that beyond 435 ^{0}C there is no weight loss for the synthesized Fe_3O_4 NPs and the nanoparticle is thermally stable. The temperature beyond which the weight loss is insignificant was used for the calcination of the synthesized Fe_3O_4 nanoparticles (Herlekar *et al*., 2015). Calcination was performed at 435°C to remove unwanted remnants of the raw materials and improve the purity of Fe_3O_4 nanoparticles.

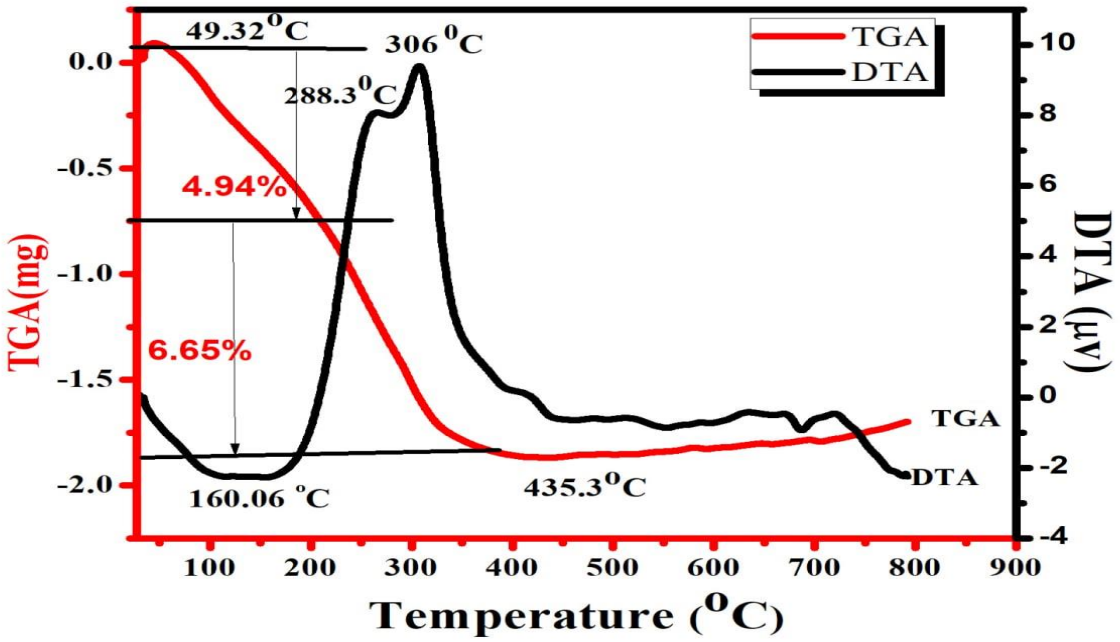

Figure 9: The TGA-DTA plots of uncalcined magnetite nanoparticles.

According to (NuchareeNucharee Chomchoey, 2018) the synthesized magnetic NPs dried in an oven at 80 °C are black and strongly attracted by a laboratory bar magnet. These magnetic NPs with magnetic behavior are most probably magnetite (Fe_3O_4). So the present study also confirmed this study which means, that the synthesized magnetite (Fe_3O_4) nanoparticle that was synthesized by chemical and green methods was attracted by a laboratory bar magnet. This magnetic NP (MNP) with magnetic behavior is most probably a magnetite (Fe_3O_4) nanoparticle.

4.1.2. X-ray Diffraction (XRD) Analysis

X-ray diffraction is a convenient method for determining the average size of single-crystal nanoparticles or crystallites in nano crystalline bulk materials (Holzwarth & Gibson, 2011). It is also an effective technique to identify the phase and confirm the crystal structure of the synthesized iron oxide nanoparticles. Figure 10 (a, b and c) shows the XRD diagrams of Fe_3O_4 NPs green synthesized from ferric chloride hexahydrate and ferrous tetra hydrate precursors and P. *julifera* leaf extract with a 1:1, 1:2, and 2:1 ratios, respectively. As shown in Figure 10 the formation of Fe_3O_4 nanoparticles was analyzed by x-ray diffraction. The diffraction peaks of the synthesized Fe_3O_4 nanoparticles (Figure 10a) Fe_3O_4 (1:1) were detected at $2\Theta = 30.16^{o}$, 34.51^{o},

35.49 ^{o}, 43.16 ^{o}, 57.02 ^{o}, and 62.71 ^{o} are assigned to the crystal planes of (220), (311), (222), (400), (511) and (440) respectively. Again as shown in (Figure 10b), for Fe_3O_4 (1:2) NPs the peak was observed at 2Θ = 30.16 ^{o}, 35.52 ^{o}, 43.16 ^{o}, 57.07 ^{o}, 57.58 ^{o,} and 62.71^{o} corresponding to the miller index values of (220), (311), (222), (400), (511) and (440), respectively. And also that of Fe_3O_4 (2:1) NPs shown in Figure 10c, the peaks were observed at 2Θ = 27.21 ^{o}, 34.63 ^{o}, 35.56 ^{o}, 46.82 ^{o}, 56.53 ^{o,} and 61.68 ^{o}C, which are assigned to the crystal planes of (220), (311), (222), (400), (511) and (440), respectively. The reason for shift of 2Θ position, the shortest peak, and small intensities of 2:1 ratio than a ratio of 1:1 and 1:2 ratio is that, due to it contains a high amount of plant extract than salt precursors or the effect of phytochemicals constituents those found in plant leaf extract during synthesis of a nanoparticle. The analyzed diffraction peaks were matched well with the standard magnetite XRD patterns (JCPDS Card No.75 - 1533), which identifies the crystallographic systems of cubic structure. Those results reveal that the green synthesis NPs possessed good crystallinity in nature and also diffraction peaks related to impurities were not observed in the XRD pattern, confirming the purity of the green synthesized nanomaterials. The average crystalline size of the green synthesized Fe_3O_4 NPs within 1:1, 1:2, and 2:1 ratios were found to be 16, 19, and 14 nm respectively. Estimation of the crystallite size of synthesized Fe_3O_4 NPs can be calculated by using the Debye- Scherrer equation, $D = k\lambda /\beta\cos\theta$ (Yuvakkumar and Hong, 2014). Figure 10 (d) the formation of iron oxide nanoparticles was analyzed by x-ray diffraction. The diffraction peaks were in good agreement with the one which was reported (JCPDS Card No.75- 1533). The peaks were observed at 2Θ = 30.27 ^{o}, 35.6 ^{o}, 37.1, 43.2 ^{o}, 57.2 ^{o,} and 62.8 ^{o} with miller indices values of (220), (311), (222), (400), (511) and (440) respectively. A similar result reported that Fe_3O_4 nanoparticles were synthesized using ferric chloride and ferrous chloride precursor. The reflection peak position and relative intensities can approximatel matched with the standard magnetite of Fe_3O_4 at 2Θ = 35.481 ^{o} confirm the inverse cubic spinel structure and the average crystallite size were calculated to be 10.6 nm (Jing *et al.,* 2007).

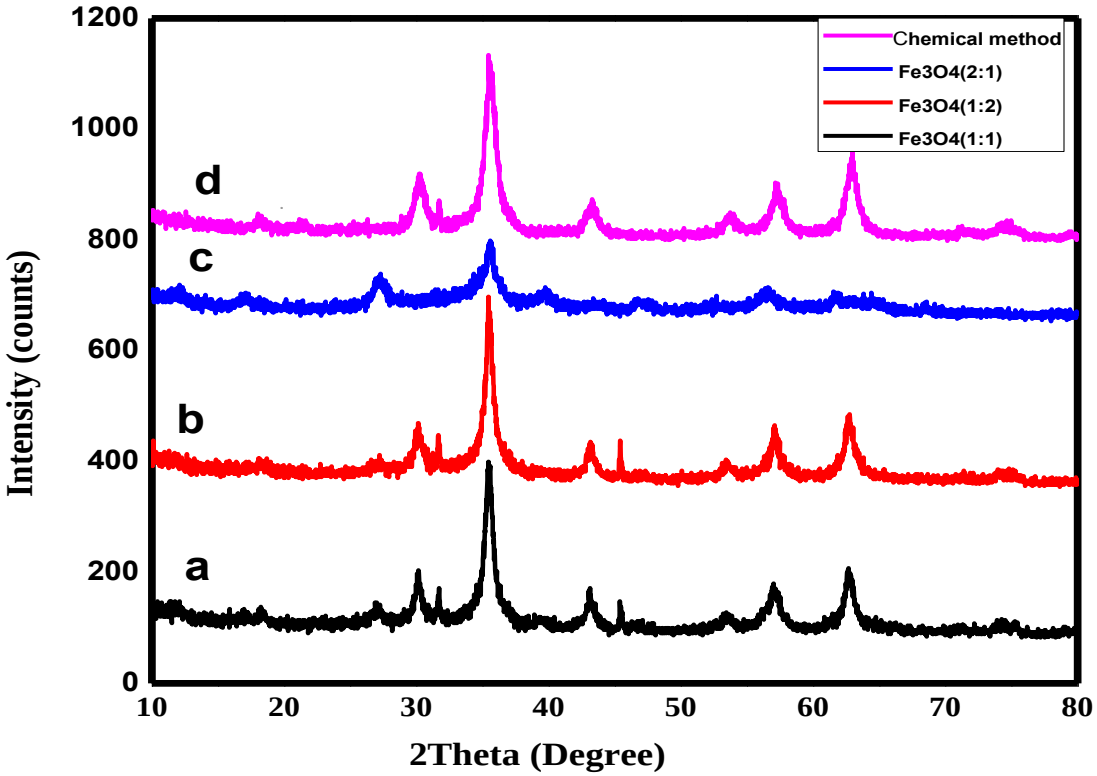

Figure 10: XRD Spectrum of green synthesized Fe_3O_4 NPs within a (1:1), b (1:2), c (2:1), and d (chemically synthesized Fe_3O_4 NPs).

The crystalline sizes of green synthesized Fe_3O_4 nanoparticles at different ratios were different from each other by depending on taking various amounts of salt precursor and plant extracts used that might result in nanoparticles with different sizes, shapes and morphologies even though the three Fe_3O_4 NPs of different proportions were prepared by the same procedure, there is a slight shift of 2θ position for certain peaks. As compared to Fe_3O_4 nanoparticles green synthesized within a 1:1 ratio**,** XRD data result showed that the average crystalline size of Fe_3O_4 nanoparticles green synthesized within a 1:1 ratio has a relatively smaller particle size (16 nm) as compared to the average crystalline size of 1:2 ratio (19 nm). This difference may be because the greater amount of P. *julifera* ef extract used during the synthesis process results in a more capping agent that in turn effectively stabilize the green synthesized Fe_3O_4 (1:1) nanoparticles. The average crystalline size of 1:2 is greater than that of 1:1, this may be due to the biological molecules entered into the metal oxide matrix being in excess, which in turn results in the formation of aggregated nanoparticles. Tables 6 and 7 are indicating different angles, FWHM

values, lattice plane, lattice parameter, and sizes of Fe_3O_4 nanoparticles for 1:1, 1:2, and 2:1 ratios by chemical method.

Table 6: Different angles, Hkl, FWHM values, and sizes of Fe_3O_4 nanoparticles for 1:1and 1:2 ratios.

Fe_3O_4 NPs (1:1)					Fe_3O_4 NPs (1:2)				
Peak numbers	2θ	Hkl	FWHM (in rad)	size (nm)	Peak numbers	2θ	Hkl	FWHM (in rad)	size (nm)
1	30.16	220	0.6233	17.3	1	30.1564	220	0.6533	16.5
2	34.51	311	0.6	18.2	2	35.5245	311	0.6943	15.8
3	35.49	222	0.742	14.7	3	43.1668	222	0.67	16.7
4	43.16	400	0.66	17.0	4	57.0779	400	0.575	20.6
5	57.02	511	0.84	14.1	5	57.5852	511	0.5066	23.5
6	62.71	440	0.735	16.6	6	62.7134	440	0.78	15.6
Average crystallite size = 16nm					Average crystallite size = 19nm				

Table 7: Different angles, Hkl, FWHM values, and sizes of Fe_3O_4 nanoparticles for 2:1 and chemical synthesis method.

Fe_3O_4 NPs (2:1)					Fe_3O_4 NPs (Chemical method)				
Peak numbers	2θ	Hkl	FWHM (in rad)	Size	Peak numbers	2θ	Hkl	FWHM (in rad)	size (nm)
1	27.2173	220	0.92	11.68	1	30.273	220	0.94	11.51
2	34.6382	311	0.92	11.89	2	35.6114	311	0.9817	11.18
3	35.5607	222	0.9667	11.35	3	37.116	222	0.72	15.31
4	46.8298	400	0.6	18.98	4	43.2467	400	0.97	11.59
5	56.5306	511	1.09	10.88	5	57.2703	511	0.97	12.27
6	61.6838	440	0.64	19.01	6	62.8809	440	1.025	11.95
Average crystallite size = 14nm					Average crystallite size = 12nm				

4.1.3. Fourier Transform Infrared (FTIR) Analysis

Fourier transform infrared (FTIR) analysis was carried out to identify the possible interaction between the biomolecules and iron ions during the reduction reactions. This FT-IR gives information on the vibration and rotational modes of motion of a molecule. Hence FT-IR is an important technique for the identification and characterization of a substance (Smith *et al*., 1998). FT-IR spectrum of the *Prosopis julifera a* leaf extract was recorded to identify the functional groups of the phyto constituents responsible for the reduction of the metal precursors. Figure 11 shows the FT-IR spectrum of plant leaf extract showing peaks at 3403.9, 2916.5, 2367.5, 1636.9, 1433.4, 1027.1, 661.3, 539.7, and 418.1, respectively. From those indicated peaks, the broad absorption peak of plant leaf extract observed at 3403.9 cm^{-1} represents the presence of O-H stretches. The absorption peak indicated at 1636.9 cm^{-1} represents the C=O stretching. The peaks at 1433.4 cm^{1} were attributed to the vibration of the double covalent bond in -CH=CH-. The peaks at 418 cm^{-1} are attributed to the vibration of the bond in the metal oxide compound.

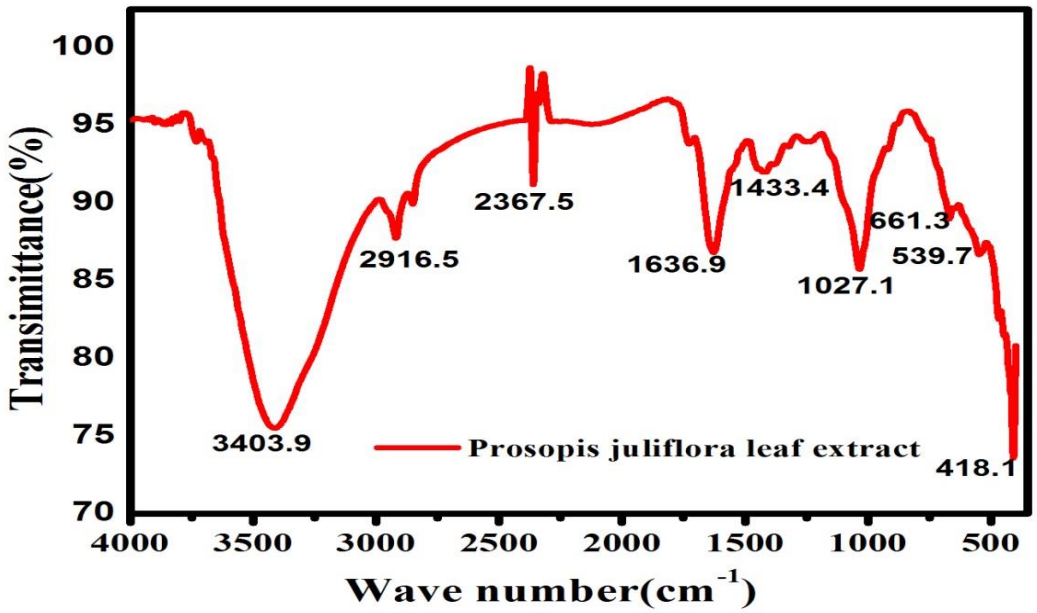

Figure 11: FT-IR plot of *Prosopis julifera* leaf extract.

The vibrational phenomenon and the quality of Fe_3O_4 NPs were also characterized by Fourier transformed infrared (FT-IR) spectroscopy in the wave number range of 500-4000 cm^{-1}.

The FT-IR spectrum of Fe_3O_4 nanoparticles is presented in Figure 12 showing the FT-IR spectra of green synthesized Fe_3O_4 (spectra A) for calcinated, (spectra B) indicate before adsorption of Fe_3O_4 nanoparticles and (spectra C) shows Fe_3O_4 after adsorption, respectively. The FTIR spectrum of green synthesized iron oxide magnetite nanoparticles showed peaks at 3439, 1618, 1088, and 554 cm^{-1}, respectively for spectra A. From those indicated peaks, the absorption peak of iron oxide nanoparticles observed at 3439 cm^{-1} represents the presence of O-H stretches due to the absorbed water on the surface of the samples. The absorption peak indicated at 1618 represents the C=O stretching. The peaks at 1088 cm^{-1} are attributed to the vibration of the C-O bond and the peaks at 539 cm^{-1} represent the peak of the Fe-O bending mode of vibration which confirms the formation of metal-oxygen bonding as reported earlier (Gotic *et al.*, 2009) which indicated the formation of Fe_3O_4 nanoparticles.

Figure 12 (B) shows the FT-IR spectrum of Fe_3O_4 NPs before adsorption showed peaks at 3355, 1600, 1369, 1040, and 591 cm^{-1}. The broad absorption peaks of magnetite nanoparticles observed at 3355 cm^{-1} indicate the presence of alcohols, and phenols with O-H stretches. The peaks at 1600, and 1369 cm^{-1} are attributed to the vibration of the double covalent bond in -CH=CH, 1040 cm^{-1} indicates the presence of C-O stretches, and the peaks at 591 cm^{-1} represent the peak of the Fe-O bending mode of vibration which confirms the formation of metal-oxygen bonding. Figure 12 (C) shows the FT-IR spectrum of Fe_3O_4 NP with peaks at 3439, 2888, 1330, 1618, 1088, and 554 cm^{-1}. The broad absorption peaks of magnetite nanoparticles observed at 3438 cm^{-1} indicate the presence of O-H stretches. The peaks at 1618, and 1330 cm^{-1} are attributed to the vibration of the double covalent bond, 1060 cm^{-1} indicates the presence of C-O stretches and the peaks at 554 cm^{-1} represent the peak of the Fe-O bending mode of vibration which confirms the formation of metal-oxygen bonding. The functional groups introduced in the nanoparticle production process indicated that biochemical compounds from P. *julifera* leaf extract decorated the surface of biosynthesized nanoparticles and enhance the interactions with water molecules resulting in more stable colloids. The result revealed that the carbonyl group from water-soluble heterocyclic compounds such as flavonoids, and alkaloids were mainly responsible for the reduction and stabilization of NPs. This suggests that the molecules in P. *julifera* leaf extract could perform the dual function of formation and stabilization of iron nano particles in the aqueous medium**.**

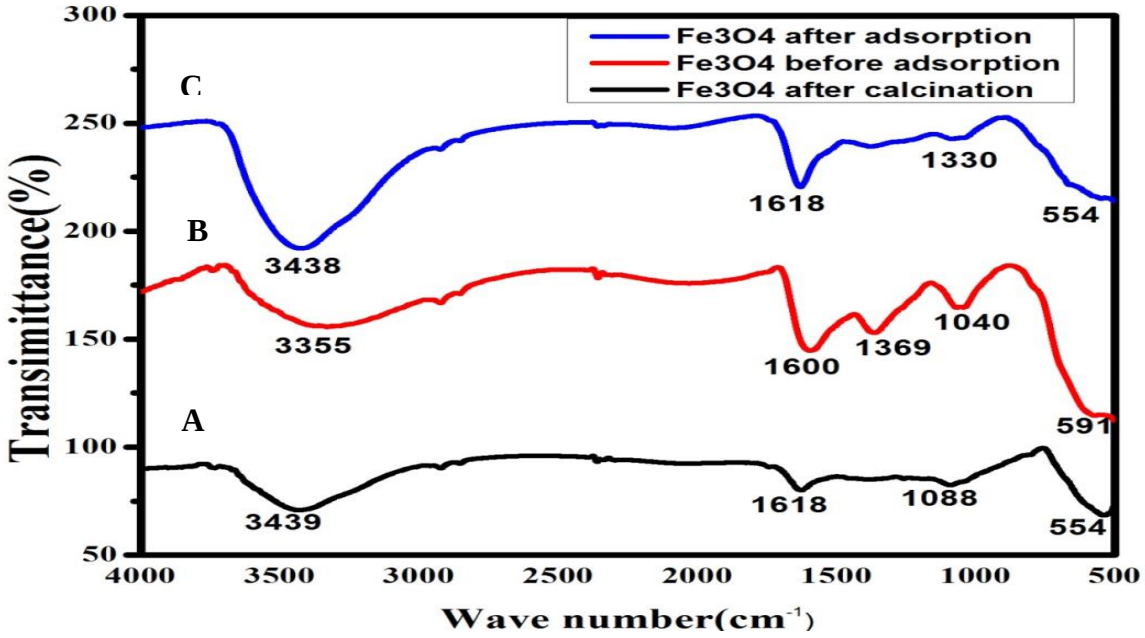

Figure 12: FTIR spectrums of Fe_3O_4 nanoparticles synthesized by green method (after calcination (A), before adsorption (B) and after adsorption (C)) of methylene blue dye.

The FT-IR spectrum of green synthesized magnetite nanoparticles before and after adsorption showed a shift in wave number and intensity difference due to different functional groups being adsorbed by MB dye after adsorption. Generally, it can be seen that the presence of different amine groups, carboxylic acids, and the alcohol found in the leaf of P. *julifera* can lead to the formation of Fe_3O_4 nanoparticles through stabilization and capping agents, respectively.

Figure 13 (A) shows the FT-IR spectrum of chemically synthesized Fe_3O_4 NPs before adsorption showing peaks at 3420, 1628, and 535 cm^{-1} respectively. From those indicated peaks, the broad absorption peak of iron oxide nanoparticles observed at 3420 cm^{-1} represents the presence of alcohols, and phenols with O-H stretch on the adsorbent surface. The absorption peak indicated at 1628 cm^{-1} represents the C=O stretching of primary amide or to C=C groups of aromatic rings. The peaks at 1313.6 cm^{-1} were attributed to the vibration of the double covalent bond in -CH=CH- and from those indicated peaks, the absorption peak of iron oxide nanoparticles was observed at 535 cm^{-1}. Figure 13 (B) shows the FT-IR spectrum of chemically synthesized Fe_3O_4 NPs after adsorption (after adsorbed by MB dye) showed peaks at 3429, 1610, 900, and 554 cm^{-1} respectively. From those indicated peaks, the broad absorption peak of iron oxide nanoparticles observed at 3429 cm^{-1} represents the presence of alcohols and phenols with O-H stretch. The

absorption peak indicated at 1610 cm^{-1} represents the C=O stretching of primary amide or to C=C groups of aromatic rings. The peaks at 1313.6 cm^{-1} were attributed to the vibration of the double covalent bond in -CH=CH- and from those indicated peaks, the broad absorption peak of iron oxide nanoparticles was observed at 535 cm^{-1}. The FT-IR spectrum of chemically synthesized magnetite before and after adsorption showed a shift in wave number and intensity.

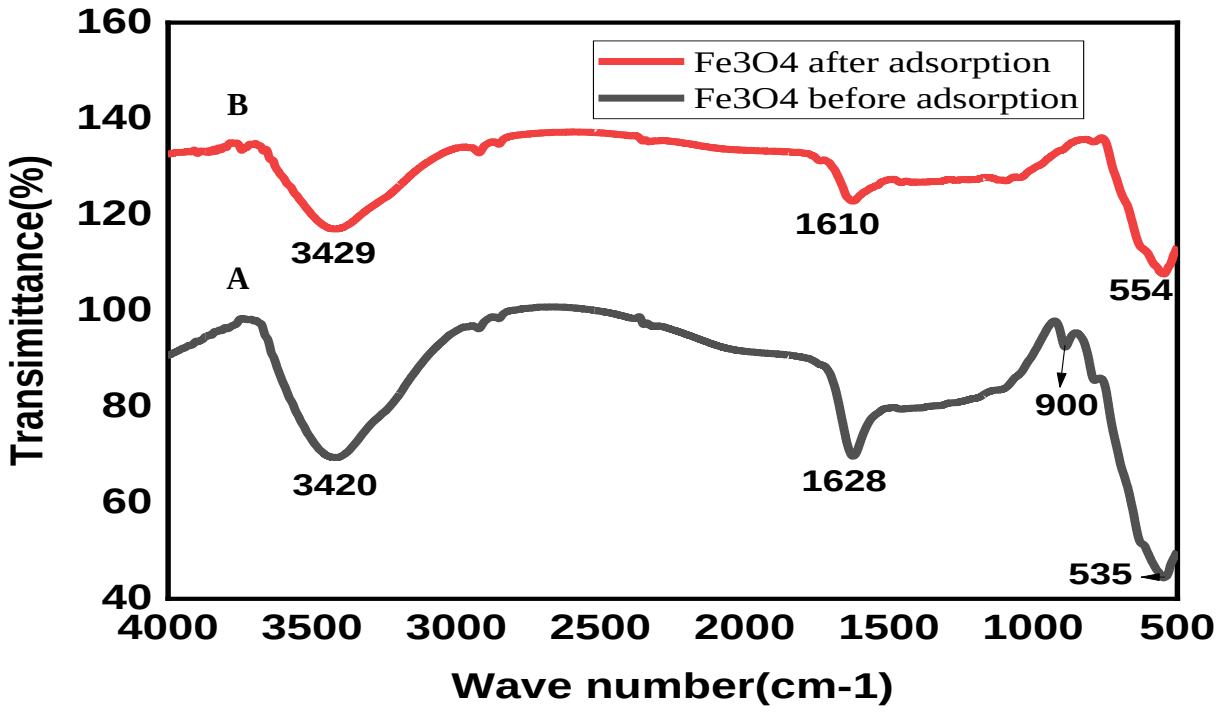

Figure 13: FTIR spectrum of Fe_3O_4 nanoparticles synthesized by chemical method (before adsorption and after adsorption) of methylene blue dye.

4.1.4. Ultraviolet-Visible Spectroscopy (UV-Vis) Analysis

UV-Visible spectroscopy is one of the most important techniques to determine and evaluate the formation and stability of metal nanoparticles in an aqueous solution. Iron oxide nanoparticle was prepared by using the aqueous leaves extract of P. *julifera* and chemical method. The formation of the nanoparticles was observed to be rapid as indicated by the color change which occurred immediately after the addition of the leaves extract to the salt precursor. The optical absorption property of Fe_3O_4 NPs powders that were synthesized by both chemical and green methods was analyzed by the absorption measurements. The absorption spectrum of sample Fe_3O_4 NPs indicates a sharp increase of the absorption in the range of 200-800 nm, typically for

Fe_3O_4 nano powders with a reddish-brown color in both green and chemical method, especially in the green method due to the addition of leaf extract to a salt precursor. The UV- Visible absorption spectra of Fe_3O_4 nanoparticles green synthesized and chemically synthesized are indicated in Figure 14 (a, b, c and d) revealing the reduction process and formation of nanoparticles. Here the sharp peak at 318,4 nm, 319 nm, and 318 nm indicates the presence of magnetite (Fe_3O_4) nanoparticles synthesized by the green method (1:1, 1:2, and 2:1) and 315 nm indicates the presence of iron oxide nanoparticles that synthesized by chemical method (co-precipitation method).

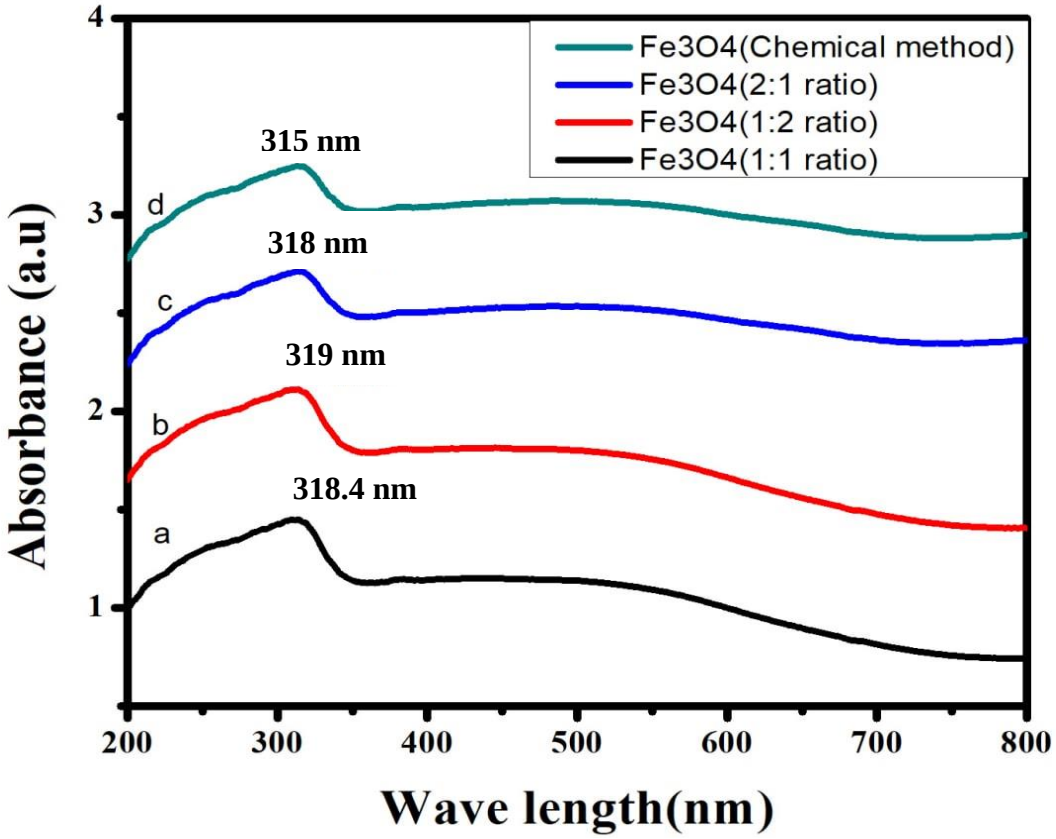

Figure 14: Figure DRS-UV- Visible Absorption of Fe_3O_4 nanoparticles.

The outer electron of the materials in their atomic state absorbs the radiant energy and undergoes the transition to a higher energy level. The energy band gap of the nanomaterial was obtained from equation, which are 3.11, 3.09, 3.13 eV for green synthesized Fe_3O_4 by 1:1, 1:2, and 2:1 ratio for average crytaine size for magnetic nanoparticles of 16 nm, 19 nm and 14 nm as

indicated in Figure 15 A, B and C as well as 3.2 eV for chemical synthesized Fe_3O_4 as indicated in Figure 15 D.

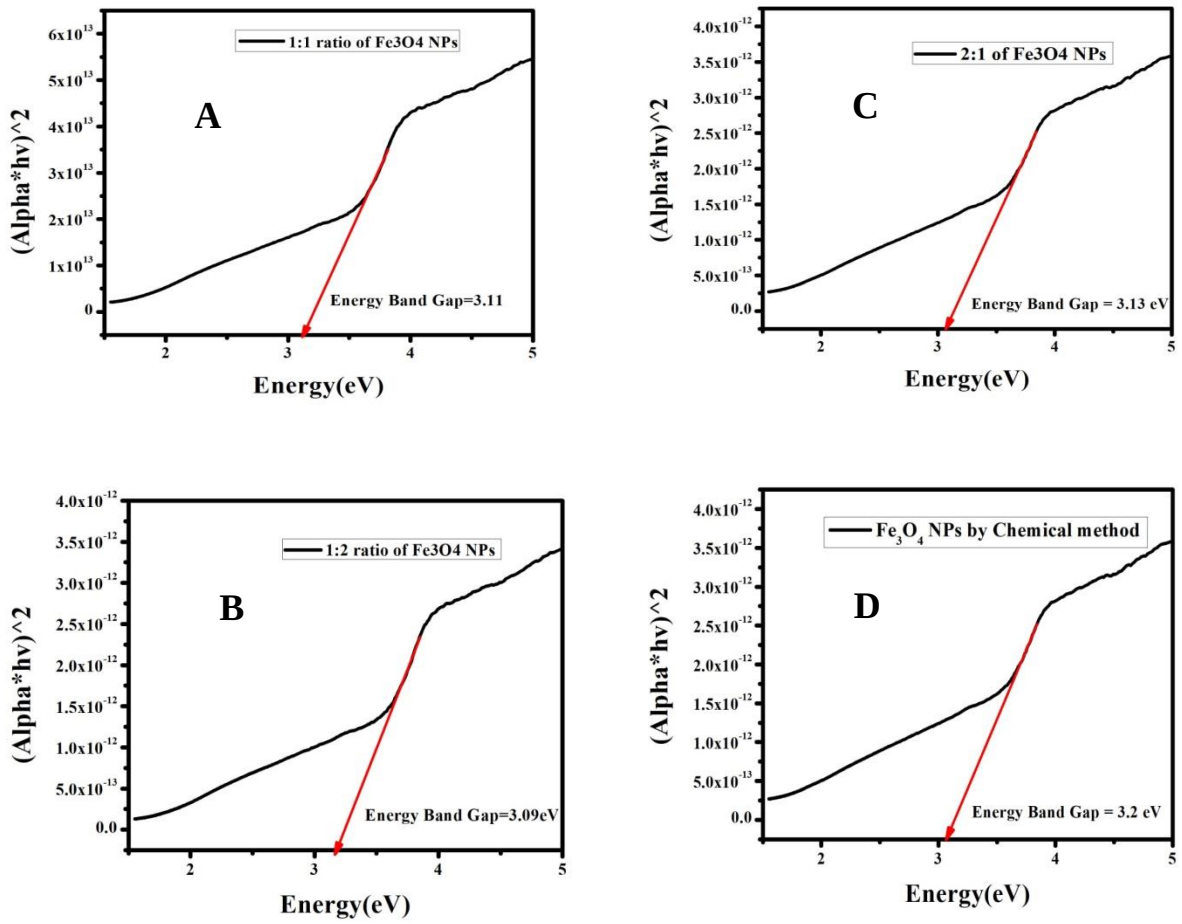

Figure 15: Energy band gap of Fe_3O_4 nanoparticles (A (1:1), B (1:2) and C (2:1), and D (chemical method)).

These results show that the energy band gap of Fe_3O_4 nanoparticles (NPs) may depend on their particle size. This can be explained quantum mechanically as the particle size reaches the nanoscale, the number of overlapping orbitals or energy level decreases, and the thickness of the band becomes thinner. This is leading to a rise in the energy band gap between the valence band and the conduction band (Madan Singha, 2018). The band gap energy was determined based on the numerical derivative of the optical absorption coefficient. The fundamental absorption method refers to the valence band to the conduction band obtained by using the energy relation formula which is $Eg = hc/\lambda$. As the nanoparticle's size changes, the color of the solution also

changes (Bhosale et al., 2014). So UV-Visible absorption spectrum is quite sensitive to the formation of nanoparticles.

4.1.5. Scanning Electron Microscopy (SEM) Analysis

Scanning electron microscopy is one of the most widely used techniques for the characterization of nanomaterials and nanostructures. The surface morphology and size of particles were determined by scanning electron microscopy (SEM) analysis. Differences in SEM images were observed between the surface topography of magnetite NPs that synthesized by chemical (A and C) and green method (B and D) before and after adsorption were observed, respectively as indicated in Figure 16. The Scanning Electron Microscopy (SEM) technique was used to observe the surface physical morphology of magnetite nanoparticles.

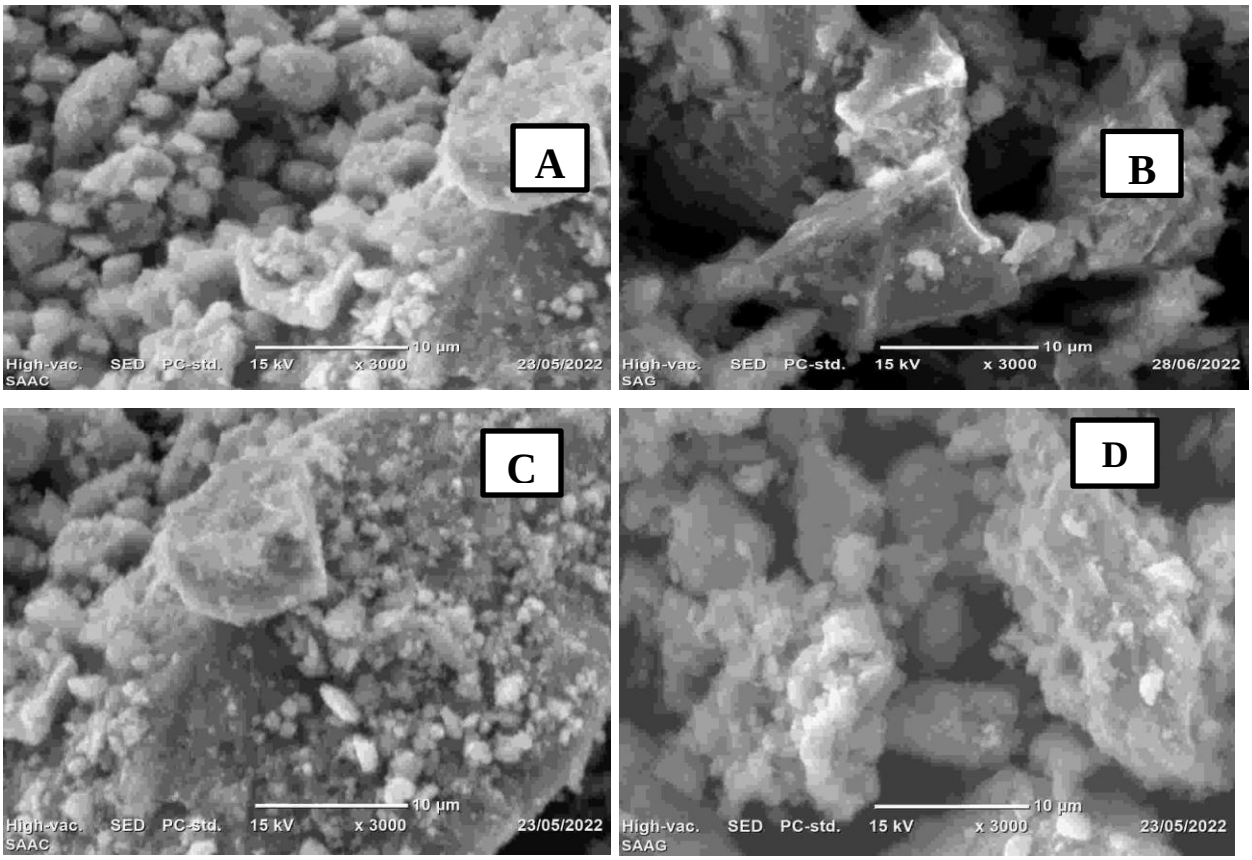

Figure 16: SEM analysis of magnetite (Fe_3O_4) by chemical (before adsorption (A) and after adsorption (C)) and by Green method (before adsorption (B) and after adsorption (D)) of MB dye.

The micrographs before and after adsorption for removal of methylene blue on the surface of the adsorbent material by both methods are given in Figure 16. The SEM image of the adsorbent before adsorption shows unoccupied pores of various sizes and shapes on the adsorbent shown in Figures 16 (A and B) for the chemical and green methods, respectively. These features favor the easy penetration of the adsorbate onto the surface of the adsorbent but after adsorption, there is an emphatic change such as a reduction in the size of some pores, disappearance of some pores, and disappearance of corners or edges in both methods. As seen in Figures 16 (C and D) the outer pores are covered by adsorbate and the pores are no longer visible. These reveal the adsorption of methylene blue on the surface of the Fe_3O_4.

4.2. Effect of Adsorption Parameters

Various factors influence the adsorption capacity of potential adsorbents during the adsorption process. The efficiency of any adsorbent is strongly influenced by the physicochemical characteristics of the solutions such as pH, initial concentration, contact time, and adsorbent dosage. Higher adsorption capacities can be obtained by optimizing the above parameters (Hua *et al*., 2012).

4.2.1. Effect of pH

It is well known that pH is one of the most important factors that affect the adsorption process of dye in water samples. The pH value of the solution is increased with an increase in the adsorption of methylene blue. Determination of the maximum pH at maximum methylene blue removal was found by adjusting the pH by using 0.1M HCl or NaOH. 0.5 g of the same magnetite nano particle that was synthesized by both chemical and green methods were added to each of the 100 mL Erlenmeyer flask containing 50 mL of methylene blue with the same concentration of 20mg/L for each both chemical and green method. The methylene blue pH was adjusted from 3 to 11 in an increment of 2 units. The mixture was shaken at 250 rpm, 20 mg/L for 60 min is equilibrium exposure time, and at room temperature, the final pH results were recorded after the equilibrium had been reached. The sample was filtered using a vacuum filter and the methylene blue concentration in the filtrate was also measured. The effect of pH on the removal efficiency of MB dye was examined over the range of pH of 3 – 11 keeping all the

parameters constant with an optimum adsorbent dosage of 50 g, contact time of 60 min, and 20 mg/L of MB dye. The plot of percentage removal versus pH and qe (mg/g) versus pH were constructed using a fitted empirical cumulative function plot to clearly understand the trend in Figure 17 and Figure 18 respectively, which shows that the percentage removal increases to pH from 3-9 and decreases on pH of 11 and adsorption capacity also increases from pH of 3-9 and decreases on pH of 10 by both magnetite nanoparticles (NPs) synthesized by both chemical and green methods, respectively. Both the removal efficiency and adsorption capacity are high in the green method rather than in the chemical method. Percentage of removal efficiency (R%) and adsorption capacity, qe (mg/g) are 97.54 % and 1.95 mg/g respectively, for green synthesized magnetite and 95.29 % and 1.94 mg/g of methylene blue uptake by magnetite synthesized using chemical method. Table 8 indicates the effect of pH on the removal efficiency of MB dye.

Table 8: Effect of pH on removal efficiency of MB dye

Parameter	Absorbance (a.u)		Green method		Chemical method	
pH	Green method	Chemical method	Removal efficiency (%)	Adsorption capacity (mg/g)	Removal efficiency (%)	Adsorption capacity (mg/g)
3	0.141	0.162	92.99	1.859	92.01	1.8402
5	0.117	0.142	94.23	1.8846	93.001	1.8699
7	0.092	0.122	95.45	1.909	93.998	1.889
9	0.005	0.095	97.54	1.9508	95.29	1.945
11	0.059	0.107	97.01	1.94	94.89	1.928

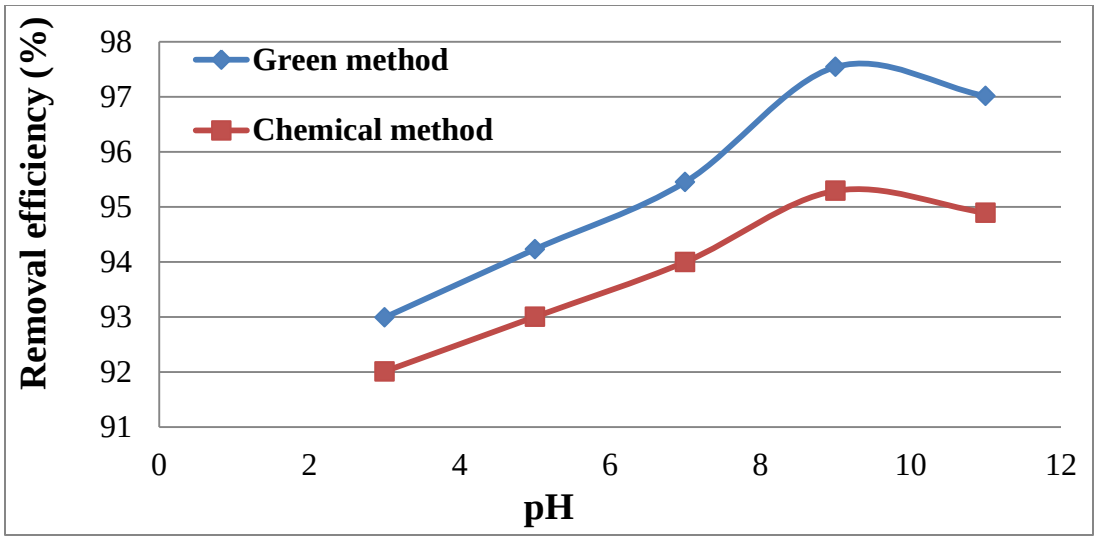

Figure 17: Effect of pH on MB dye removal by magnetite that synthesized by green and chemical method, adsorbent dose = 0.5 g/50 mL, and time = 60 min.

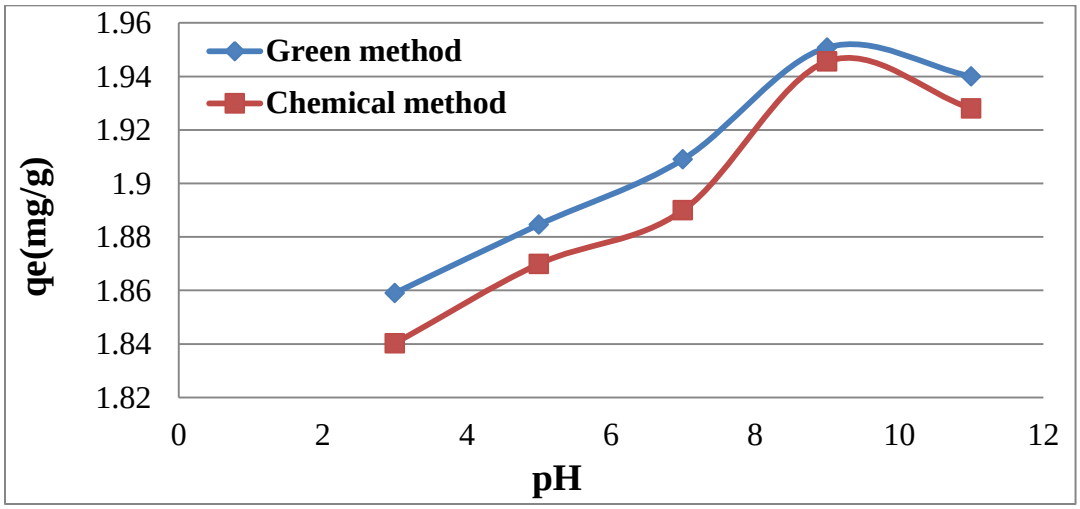

Figure 18: Effect of pH on MB dye uptake by magnetite synthesized by chemical and green method, adsorbent dose = 0.5/50mL and time = 60 min.

4.2.2. Effect of adsorbent dosage

It is well known that the effect of adsorbent dosage is the other important factor that affect the adsorption process. Several research groups have investigated the influence of adsorbent dosage by varying the adsorbent dosage concentration (Malihe Pooresmaeil, 2020). The adsorption takes place on a surface. The methylene blue (MB) removal process was found to be positively

affected by the dosage of the iron nano particle. The effect of adsorbent dosage on the removal efficiency of MB dye was examined over the range of adsorbent dose 0.1 g – 0.5 g keeping all the parameters constant with an optimum pH of 9, contact time 60 min, and 20 mg/L of MB dye. The result which is presented in Figure 19 indicates that an increase in adsorbent dose shows an increase in the percentage of removal efficiency in agreement with (Berihun, 2017) the effect of adsorbent dose on MB dye removal was studied by varying adsorbent dose from 0.1 to 0.5 g and it was seen that removal efficiency increases with increasing adsorbent dose. The change in adsorbent dose from 0.1 g to 0.5 g can increase removal from 98.01 % to 98.79 % in the green method and 97.72 % to 98.66 % in a chemical method for MB dye removal by keeping other factors constant. This trend was due to an increase in surface area and adsorption sites available for adsorption. These results indicate that removal efficiency is directly related to the number of available adsorption sites. This suggests that after a certain dose of adsorbent, the maximum adsorption sets in, and hence the amount of dyes bound to the adsorbent and the number of free ions remains constant even with further addition of the dose of adsorbent. The amount of adsorbent added to the solution determines the number of binding sites available for adsorption. Dye adsorption efficiency was increased with an increase in adsorbent dose. This implies that the adsorption sites remain unsaturated during the adsorption reaction whereas the number of sites available for adsorption sites increases by increasing the adsorbent dose. Table 9 indicates the effect of adsorbent dosage on the removal efficiency of MB dye.

Table 9: Effect of adsorbent dosage on removal efficiency of MB dye

Parameter	Absorbance (a.u)		Green method		Chemical method	
Adsorbent dosage (g)	Green method	Chemical method	Removal efficiency (%)	Adsorption capacity (mg/g)	Removal efficiency (%)	Adsorption capacity (mg/g)
0.1	0.027	0.047	98.01	9.801	97.72	9.191
1.2	0.026	0.043	98.143	4.9	97.917	4.495
0.3	0.025	0.041	98.215	3.273	98.02	3.06
0.4	0.024	0.03	98.66	2.466	98.565	2.164
0.5	0.023	0.028	98.79	1.976	98.665	1.473

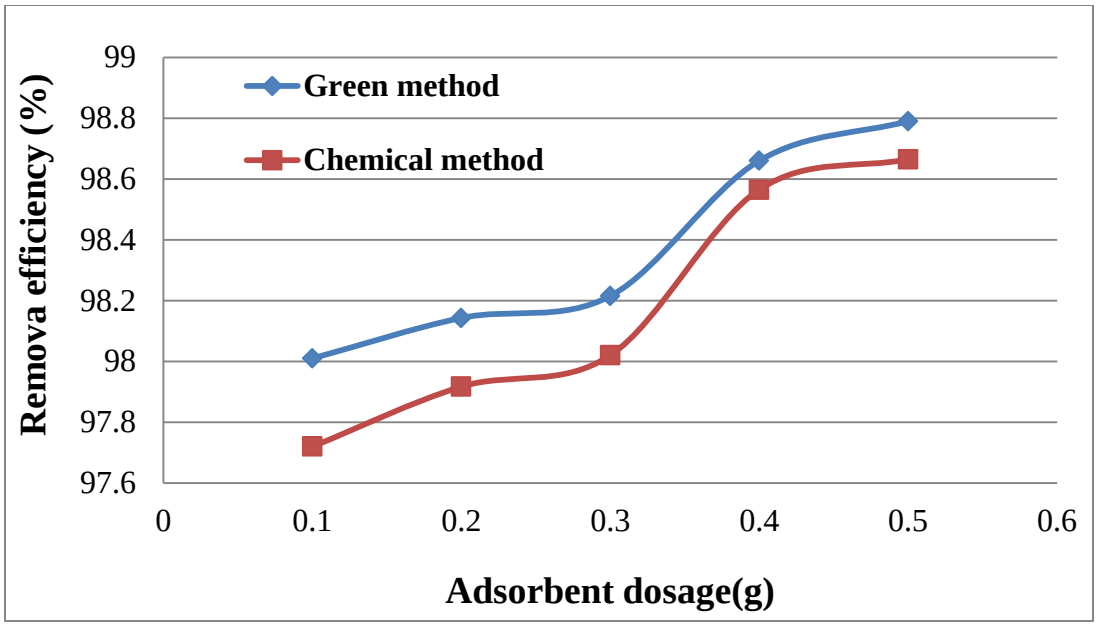

Figure 19: Effect of adsorbent dose on MB dye removal efficiency by magnetite at pH = 9 and time = 60 min and MB dye concentration = 50 mg/L.

As shown in Figure 20 the adsorption capacity of adsorbents was found to decrease with increasing adsorbent dosage as the number of adsorption sites per unit mass decreased.

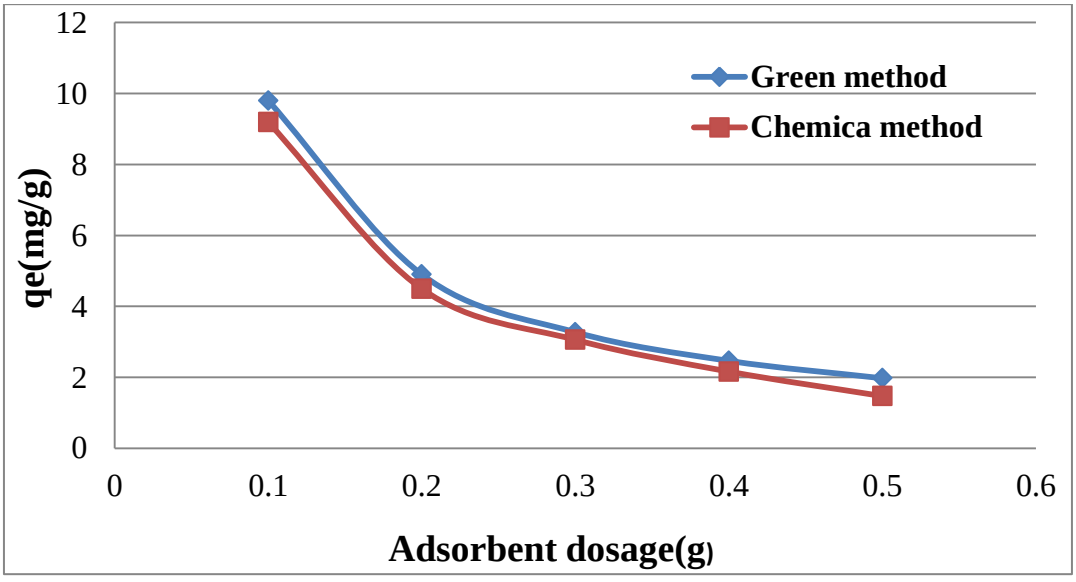

Figure 20: Effect of adsorbent dose on MB dye uptake by magnetite at pH = 9 and time = 60 min and MB dye concentration = 50 mg/L.

4.2.3. Effect of contact time

The shaking time (contact time) is another important factor in evaluating the affinity of magnetite nanoparticles to methylene blue. An adsorbent that has hydrophilic groups is defined as the most effective adsorbent (Bilgiç, 2019). In the studies of the effect of contact time on the removal of dye when the time increases the rate of adsorption also highly increases at the first stage of the adsorption process and after that the adsorption rate decrease to reach an equilibrium point. Removal efficiency for methylene blue (MB) at an exposure time of 20- 100 min with 20-minute intervals was investigated. The effect of contact time on the removal efficiency of MB dye was examined over the range of adsorbent dose 20 min – 100 min keeping all the parameters constant with an optimum pH of 9, an adsorbent dosage of 0.5 g, and 20 mg/L of MB dye. As Figure 21 shows, the optimum exposure time for methylene blue removals by magnetite iron nano particle was obtained in 60 min. Therefore, the methylene blue adsorption was found to increase with an increase in time from 20-60 min and decrease after 60 min in both methods. The change in contact time from 20min to 60 min can increase the removal efficiency from 99.16% to 99.25% as well as 98.91% to 99.35% and decrease 97.72% and 97.24% in 100 min in both green and chemical methods respectively for MB dye removal by keeping other factors at the constant. The methylene blue sorption in mentioned time was attributed to the surface junction between active surface groups and dye. Also, the further sorption at the described times can be illustrated with increased availability in the active bounding sites on the sorbent surface area. The plot of percentage removal versus exposure time for both methods was constructed at pH 9, 25 °C, and 20 mg/L using a fitted empirical cumulative function plot to clearly understand the trend that the percentage removal to exposure time increment.

As shown in Figure 22 the adsorption capacity of adsorbents was found to increase with increasing contact time from 20-60 min and decrease after 60 min especially in 100 min in both chemical and green method which indicate that increase at the first stage of the adsorption process and after that the adsorption rate decrease to reach an equilibrium point. Table 10 indicates the effect of contact time on the removal efficiency of MB dye.

As is observed in Figure 22 the amount of MB dye adsorbed on to the adsorbent increased from 1.83 mg/g to 1.996 mg/g and 1.978 mg/g to 1.987 mg/g as time increased from 20min to 60 min and decreased to 1.956 mg/g and 1.934 mg/g of adsorbent that synthesized by green and chemical method respectively taken by methylene blue for removal.

Table 10: Effect of contact time on removal efficiency of MB dye

Parameter	Absorbance (a.u)		Green method		Chemical method	
Contact time (min)	Green method	Chemical method	Removal efficiency (%)	Adsorption capacity (mg/g)	Removal efficiency (%)	Adsorption capacity (mg/g)
20	0.018	0.023	99.16	1.983	98.91	1.978
40	0.011	0.014	99.55	1.99	99.36	1.987
60	0.005	0.011	99.75	1.996	99.505	1.99
80	0.025	0.013	98.81	1.97	99.404	1.95
100	0.014	0.093	97.82	1.956	97.24	1.934

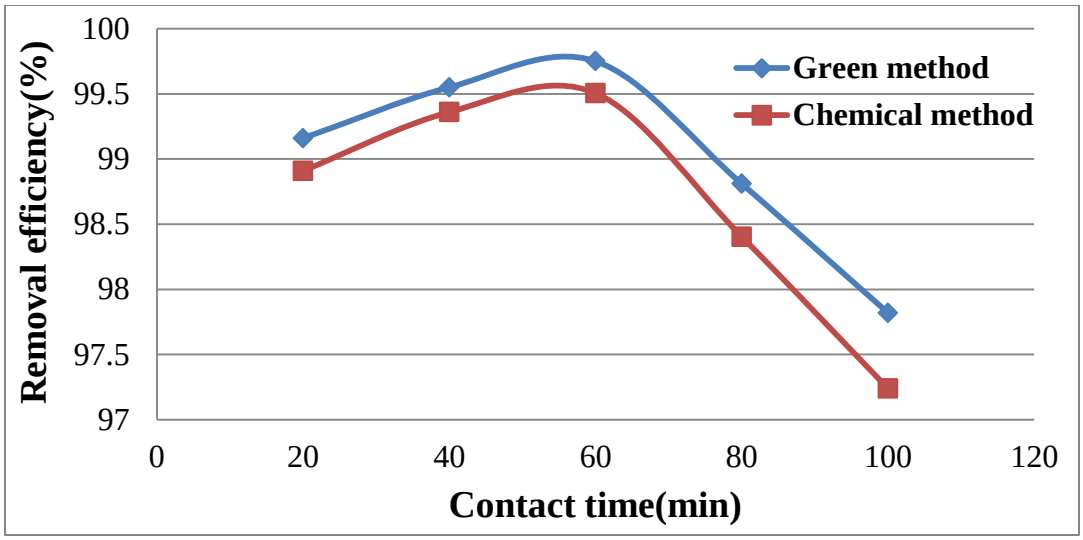

Figure 21: Effect of contact time on MB dye removal efficiency by magnetite at pH = 9, adsorbent dose = 0.5 g/50 mL and MB dye concentration = 50 mg/L.

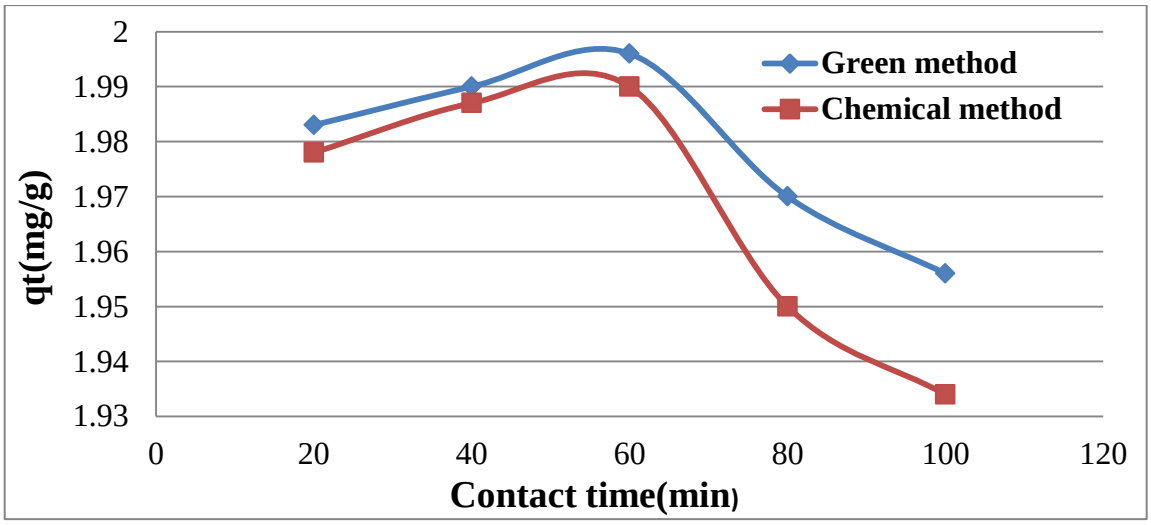

Figure 22: Effect of contact time on MB dye uptake by magnetite at pH = 9, adsorbent dose = 0.5 g/50 mL and methylene blue concentration = 50 mg/L.

4.2.4. Effect of initial concentration

The effect of the initial concentration of methylene blue on removal efficiency was investigated in the range of 10 to 50 mg/L. The adsorption process was observed to be inversely affected by the initial methylene blue concentration, the removal process decreased with increasing methylene blue concentration from 10 mg/L to 50 mg/L. As Figure 23 revealed, the removal

efficiency of methylene blue (MB) decreased as the initial concentration of methylene blue increased. The plot of percentage removal versus MB concentration was constructed at pH 9, 60 min, 25 °C, 0.5 g, and 10 mg/L using a fitted empirical cumulative function plot to clearly understand the trend that the percentage removal to methylene blue concentration increment. The Adsorption of MB dye on magnetite that was synthesized by both chemical and green methods as a function of initial was studied by the varying initial concentration of methylene blue from 10 mg/L to 50 mg/L by keeping all parameters at optimum value and the result is represented in Figure 23 and 24. It is noted that, with an increase in the initial concentration of MB dye from 10 mg/L to 50 mg/L, the percentage of removal efficiency of MB dye was decreased from 99.75% to 94.89% in the green method and 99.505% to 94.21% in the chemical method. Table 11 shows the effect of initial concentration on removal efficiency and adsorption capacity of MB dye.

Table 11: Effect of initial concentration on removal efficiency and adsorption capacity of MB dye

Parameter	Absorbance (a.u)		Green method		Chemical method	
Initial concentration (mg/L)	Green method	Chemical method	Removal efficiency (%)	Adsorption capacity (mg/g)	Removal efficiency (%)	Adsorption capacity (mg/g)
10	0.0109	0.088	99.75	0.992	99.505	0.78
20	0.027	0.067	98.04	1.96	97.49	1.755
30	0.118	0.069	96.23	2.88	97.71	2.67
40	0.115	0.086	95.378	3.803	95.04	3.601
50	0.134	0.139	94.89	4.745	94.21	4.514

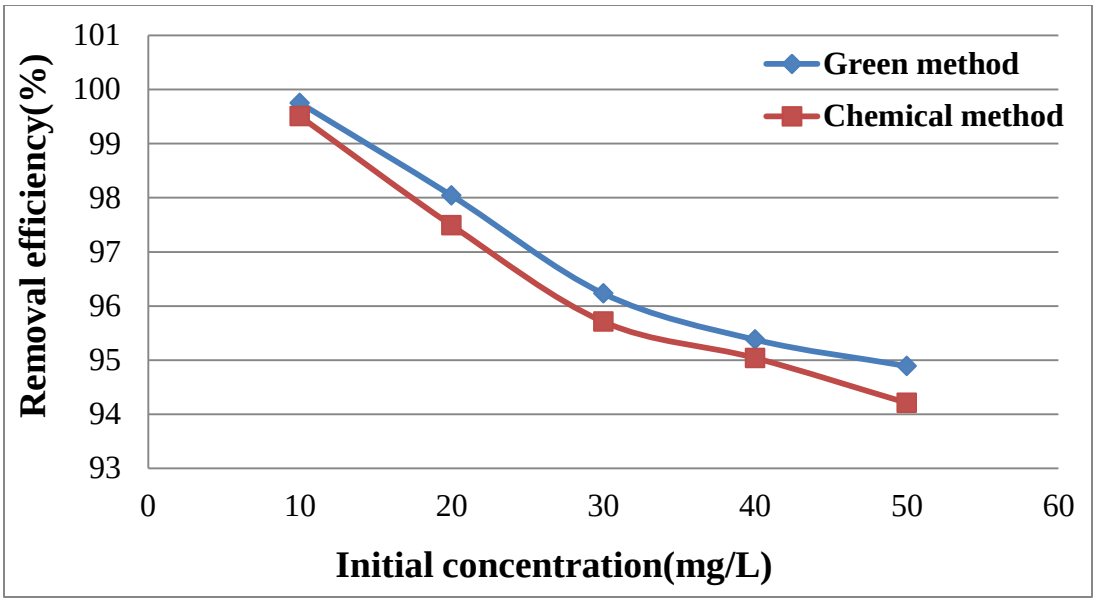

Figure 23: Effect of initial concentration on MB dye removal by magnetite at pH = 9, adsorbent dose = 0.5g/50mL and time = 60 min.

As is observed in Figure 24 the amount of MB dye adsorbed on to the adsorbent increased from 0.992 mg/g to 4.745 mg/g in the green method and 0.78 mg/g to 4.514mg/g in the chemical method with an increase in the initial concentration of MB dye from 10mg/L to 50 mg/L.

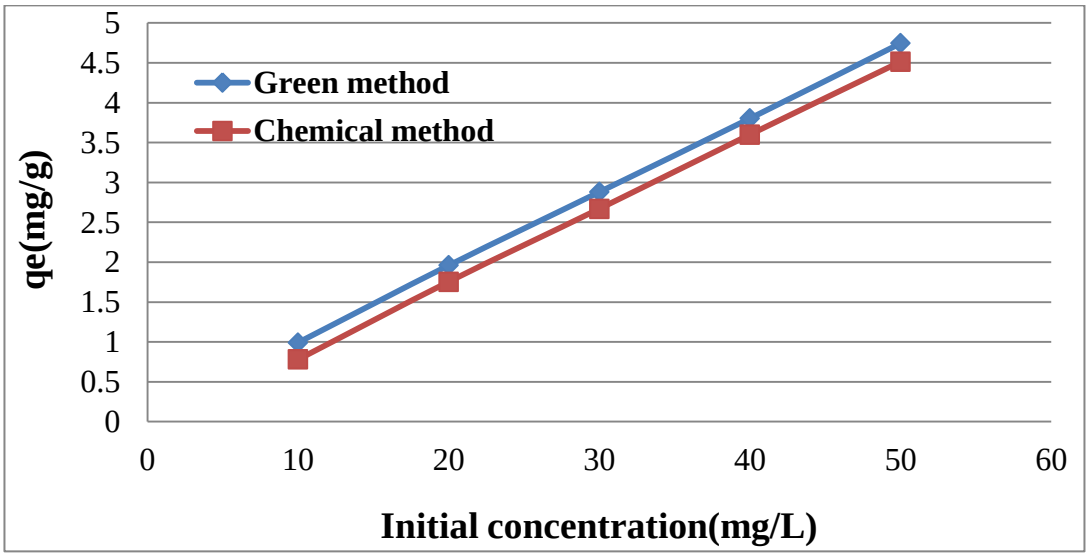

Figure 24: Effect of initial concentration on MB dye uptake by magnetite at pH = 9, adsorbent dose = 0.5 g/50mL and time = 60 min.

The percentage removal decreases with increasing initial concentration; (Hsini et al., 2021) reported that the percentage removal of MB dye decreases as the concentration of MB dye in solution is increased. This is due to less active sites being available for MB dye because their sites saturate above a certain concentration and additional adsorbate does not get adsorbed hence the percentage removal decreases (Farnam et al., 2015).

4.3. Adsorption Isotherm Result

The equilibrium data for the adsorption are commonly known as adsorption isotherms. It is essential to know them so as for comparing the effectiveness of different adsorbent materials under different operational conditions and to design and optimize an adsorption system. It is important to investigate the adsorption isotherm for the description of the capacity of adsorption. An adsorption isotherm equation is an expression of the relation between the amount of solute adsorbed and the concentration of the solute in the fluid phase since the adsorption isotherms are important to describe how adsorbate interact with the adsorbents and so are critical for design purposes (Kyzas & Kostoglou, 2014).

4.3.1. Langmuir Adsorption Isotherm

Langmuir adsorption isotherm assumes that qualitatively the formation of monolayer adsorbate on the outer surface of the adsorbent, then after no further adsorption takes place. According to this model maximum adsorption occurs when a saturated monolayer of solute molecules is present on the surface of the adsorbent, the energy of adsorption is fixed and molecules of the adsorbent will not migrate in the surface plane. As presented in Figure 25, the graph of Ce/qe Vs Ce for both chemical and green methods was plotted. K_L is the Langmuir constant, and qmax is the maximum adsorption capacity (mg g^{-1}) and calculated from intercept and slope. The removal of methylene blue by magnetite nanoparticle at different methylene blue is depicted in Figure 25 for both chemical and green methods. It was observed that the adsorption of methylene blue onto the iron oxide (Fe_3O_4) nanoparticle decreased with a rise in the concentration of methylene blue from 10 to 50 mg/L. This is attributed to the greater driving force through a higher concentration gradient at a high dye concentration. Thus, the developed iron NPs (magnetite, Fe_3O_4 can be efficiently used for the removal of high concentration methylene blue from aqueous solutions. As

the data in Table 12 shows the value of all Langmuir adsorption isotherm parameters included under both methods. The values of $K_L > 1$, $K_L = 1$, and $K_L < 1$ reflect that the adsorption is unfavorable, linear, and favorable, respectively (Jianlong Wang, 2020). For instance, K_L is 1.564 L/g and 0.0566 L/g while R_L is 0.0566 and 0.1027 in green and chemical methods respectively confirming that the sorption of MB dye on magnetite is favorable and R^2 is 0.9273 and 0.9487 in green and chemical method, respectively.

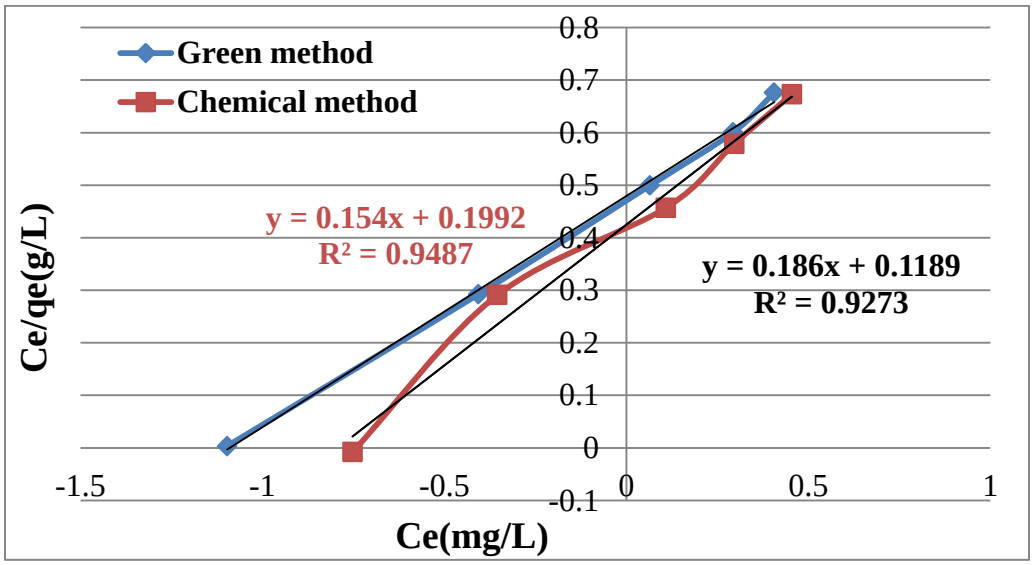

Figure 25: Langmuir adsorption isotherm model

Table 12: Langmuir adsorption isotherm parameters

	Green method	Chemical method
Qmax	5.376 mg/g	6.4935mg/g
K_L	1.564 L/g	0.775 L/g
R^2	0.9273	0.9487
R_L	0.0566	0.1027
Equation	Ce/qe = 0.186ce + 0.1189	Ce/qe = 0.154ce + 0.1992

The R_L (the separation factor) value lies between 0 and 1 which confirm that the adsorption process of MB dye is favorable on magnetite in both chemical and green method. The maximum adsorption capacity (Qmax) by magnetite determined was 15.6935 mg/g and 0.775 mg/g which

means 15.6935 mg/g and 0.775 mg/g of MB dye are absorbed by one gram of magnetite for that synthesized by green Vs chemical method respectively. The value of R_L is 0.0566 and 0.1027 in the green and chemical methods respectively which is indicate that the adsorption of MB dye on magnetite is favorable in both methods. R^2 is 0.9273 and 0.9487 in a green and chemical method which is less than R^2 value of the Freundlich adsorption isotherm, for this reason, the Langmuir adsorption isotherm parameters model does fail to describe the experimental finding.

4.3.2. Freundlich Adsorption Isotherm

To determine whether the Freundlich adsorption isotherm model fit the experimental value or not the graph of log qe as a y-axis and log Ce as an x-axis was plotted. From the linear equation, the value of K_f (adsorption capacity) and 1/n was calculated and the Freundlich adsorption isotherm equation was developed. The smaller 1/n becomes, the greater the expected heterogeneity and if n is between one and ten or 1/n was less than one, it indicates a favorable sorption process (Thiebault, 2020). Table 13 shows the value of parameters for the Freundlich adsorption isotherm model. 1/n is 0.4403 and 0.5359 while n is 2.271 and 1.866 in green and chemical methods, respectively confirming that the sorption of MB dye on magnetite iron oxide nanoparticle is favorable and R^2 is 0.9981 and 0.9838 in green and chemical method indicate that the sorption data are fitted well to Freundlich adsorption isotherm model for both methods rather than Langmuir isotherm model. Figure 26 shows Freundlich Adsorption Isotherm

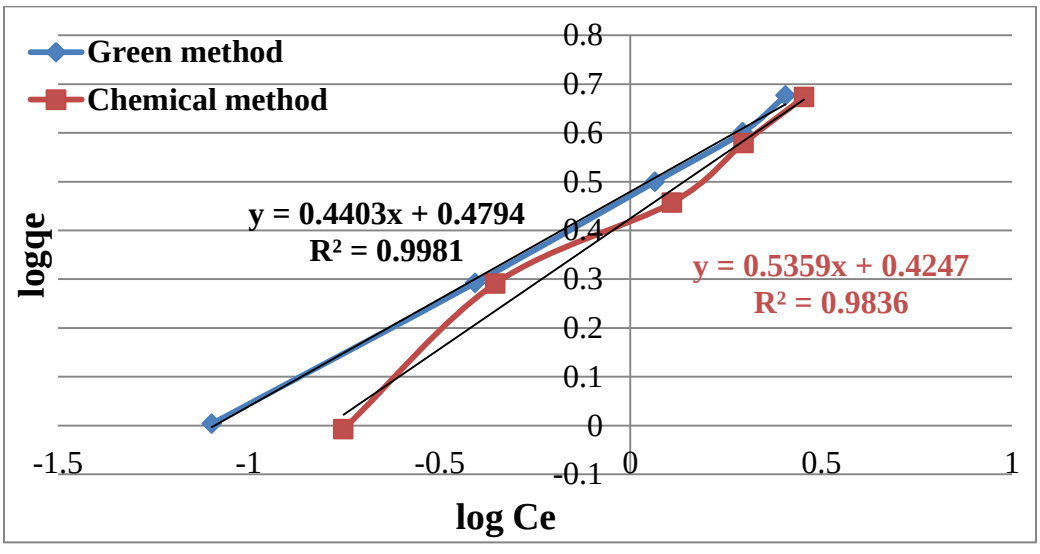

Figure 26: Freundlich Adsorption Isotherm.

Table 13: Freundlich adsorption isotherm parameters

	Green method	Chemical method
n	2.271	1.866
1/n	0.4403	0.5359
K_f	3.0157	2.658
R^2	0.9981	0.9836
Equation	Ce/qe = 0.4403ce + 0.4794	Ce/qe = 0.5359ce + 0.4247

4.4. Adsorption Kinetics studies

The effect of contact time on the amount of adsorbed MB was investigated at the initial concentration of 10 mg/L and 20 mg/L at pH 9 at room temperature. The concentration of MB was measured using a spectrophotometer. The nanoparticle adsorption was measured periodically at 20, 40, and 60 min. The Figures below shows the effect of contact time on the adsorption capacity of MB by the magnetite nanoparticles by using 10 mg/L and 20 mg/L of methylene blue concentration. It is clear that the adsorption capacity increases rapidly during the initial adsorption stage and then continues to increase at a relatively slow speed with contact time and reaches an equilibrium point after 60 min. To investigate the adsorption mechanism of MB for magnetite nanoparticles, two kinetic models, the pseudo-first-order kinetic model, and the pseudo-second-order kinetic model, were considered to find the best-fitted model for the experimental data.

4.4.1. Pseudo-First-Order Kinetics Model

To determine whether the adsorption mechanism is determined by pseudo first order or not the graph of log (qe-qt) vs. t was plotted as stated in Equation 2.8 and its linearity was observed by considering the correlation coefficient value. The values of k_1 and qe were calculated from the slope and intercept of the plot of log (qe-qt) Vs t respectively and Table 14 summarize the value of the kinetics parameters for both (green and chemical) method. The pseudo-first-order plots of MB dye adsorption on magnetite for two different concentrations (10 and 20 mg/L) are shown in Figure 27 and Figure 28 respectively for both methods. The value of R^2 for the pseudo-first-order was low as compared to R^2 value of pseudo- second order. As the data indicated in Table 14

shows the value of parameters for the Pseudo First Order Kinetics Model. For example R^2 is 0.9986 and 0.9976 for 10 mg/L and 20 mg/L in green method and 0.9973 and 0.9923 for 10 mg/L and 20 mg/L in chemical method. The lower R^2 value obtained indicates that adsorption of MB dye on iron oxide nanoparticles does not follow pseudo-first-order kinetics which means that adsorption of methylene blue dye on iron oxide nanoparticles does follow pseudo-second-order kinetics.

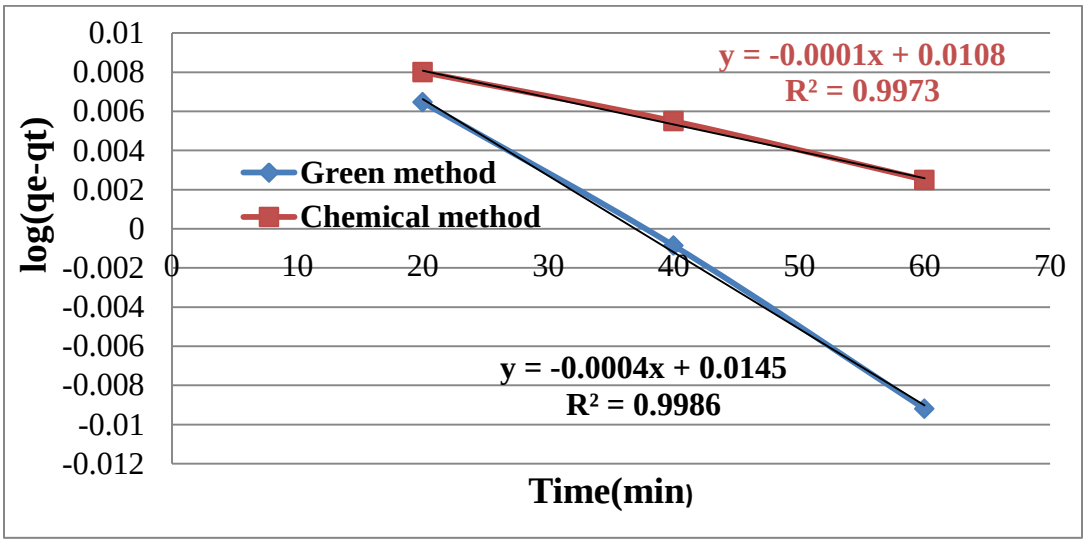

Figure 27: Pseudo first order kinetic curve at 10 mg/L.

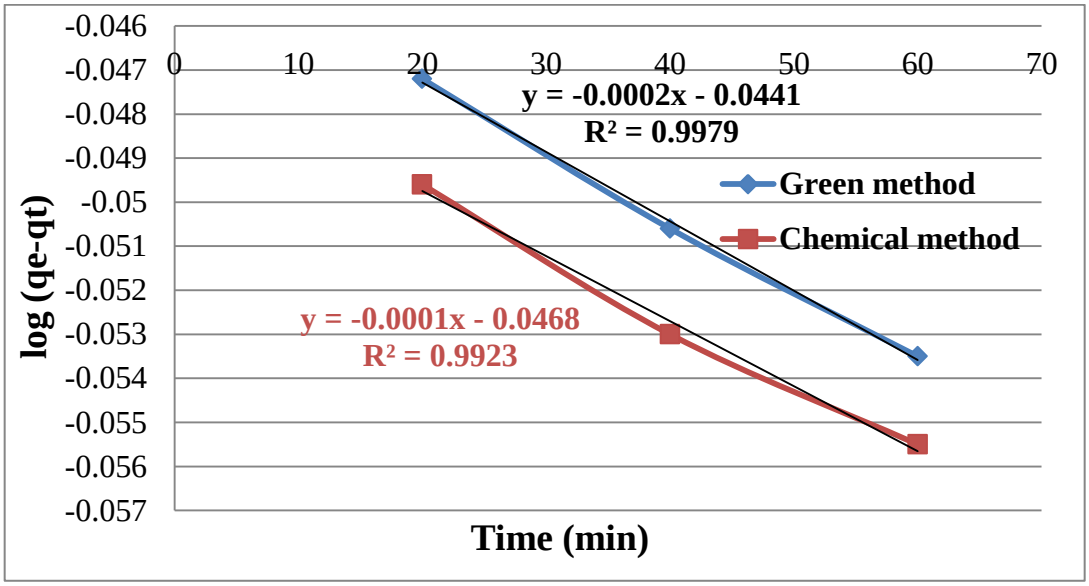

Figure 28: Pseudo first-order kinetic curve at 20 mg/L.

Table 14: Adsorption Kinetics parameters for Pseudo first order.

Contaminant	Concentration (mg/L)	Qe exp (mg/L)		Qe cal (mg/L)		K_1		R^2	
		Green method	Chemical method	Green method	Chemical method	Green method	Chemical method	Green method	Chemical method
MB dye	10mg/L	1.96	1.9558	1.0339	1.025	0.0009	0.00023	0.9986	0.9973
	20mg/L	2.88	2.87	1.1068	1.11378	0.0004	0.00023	0.9979	0.9923

4.4.2. Pseudo-Second-Order Kinetics Model

To determine whether the adsorption mechanism is determined by pseudo-second-order or not the graph of t/qt vs. t was plotted using Equation 2.9 and its linearity was observed by considering the correlation coefficient value. The values of qe and K_2 were calculated from the slope and intercept of the plot of t/qt vs. t, respectively and Table 14 summarize the value of the kinetics parameters for both green and chemical method. The pseudo-second-order plots of MB dye on magnetite nanoparticles that were synthesized by green and chemical methods for two different concentrations (10 and 20 mg/L) are shown in Figures 29 and 30, respectively for both methods. The value of R^2 for the pseudo-second-order was higher as compared to R^2 value of the pseudo-first-order in both the chemical and green methods. Table 15 shows the value of parameters for the Pseudo Second Order Kinetics Model. R^2 is 0.9999 and 0.9993 for 10 mg/L and 20 mg/L in green method respectively and 0.9997 and 0.9995 for 10 mg/L and 20 mg/L in chemical method respectively. Therefore, the pseudo-second-order adsorption model is more favorable to describe the adsorption kinetics of MB dye on magnetite (Fe_3O_4) that synthesize by coprecipitation method and green synthesizing method by using *Prosopis julifera* as reducing and capping agent with salt precursors which indicate that chemisorption is the rate-limiting step.

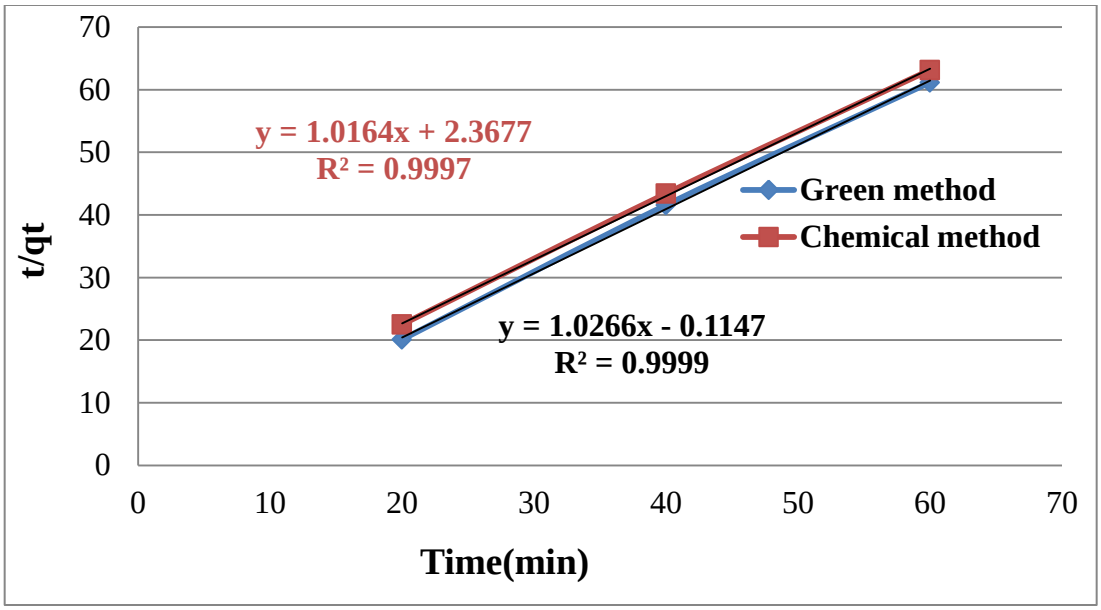

Figure 29: Pseudo second order kinetics curve at 10mg/L

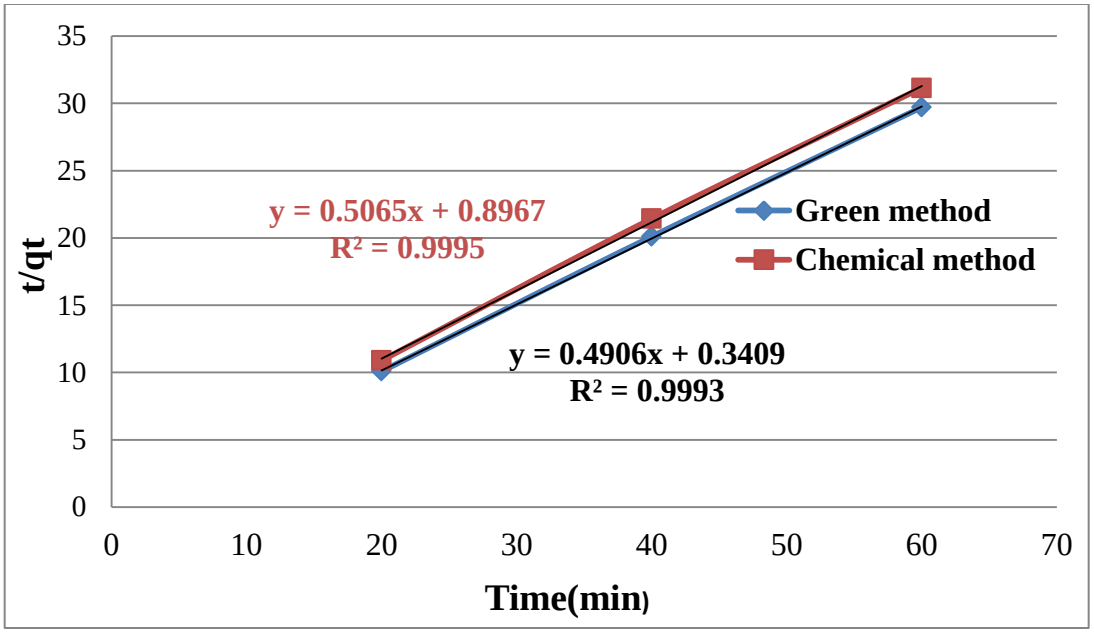

Figure 30 **:** Pseudo second order kinetics curve at 20 mg/L.

Table 15: Adsorption Kinetics parameters for Pseudo second order.

Contaminant	Concentration (mg/L)	Qe exp (mg/L)		Qe cal (mg/L)		K_2		R^2	
		Green method	Chemical method	Green method	Chemical method	Green method	Chemical method	Green method	Chemical method
MB dye	10mg/L	1.96	1.9558	0.9740	0.9838	9.1885	0.4363	0.9999	0.9997
	20mg/L	2.88	2.87	2.0383	1.9743	0.706	0.2861	0.9993	0.9995

4.5. Reusability Experiment

The regeneration and reusability of the adsorbent are important aspects to be considered for the applicability of the adsorbent in an aqueous solution. After the adsorption, the adsorbent was loaded with the methylene blue (MB) dye. Discharge of the spent adsorbent with MB dye to the environment is environmentally not good because the MB dye on the adsorbent is toxic and carcinogenic to human health and environmental pollution. Due to this reason recycling adsorbents after usage was one of the most important for reducing dyes that are discharged into the environment and water bodies. From an economical point of view, regeneration and reusability of the adsorbent are cost-saving methods. The result for this recyclability study indicates the removal efficiency of MB dye from aqueous solution by reused adsorbent for the first, second, third, fourth, and fifth cycles are indicated for both chemical and green methods, respectively as shown in Figure 31. Also, it helps to avoid the problem of adsorbent disposal which may lead to secondary pollution (Santhi, Manonmani, Smitha, & Mahalakshmi, 2009). From Table 16, the efficiency of the adsorbent for the removal of MB dye dropped from 98.3 % and 98.1 % to 84.6 % and 83.9 % by green and chemical methods, respectively after 5 consecutive usages. Overall, it can be concluded that magnetite has good regeneration and reusability potential by both methods. Table 16 indicates the removal efficiency of MB dye by magnetite adsorbent after different cycles by green and chemical methods.

Table 16: Removal of MB dye by magnetite adsorbent after different cycles (1st, 2nd, 3rd, 4th, and 5th).

No of cycle	Absorbance (a.u)		Adsorption capacity (mg/g)		Removal efficiency (%)	
	Green method	Chemical method	Green method	Chemical method	Green method	Chemical method
1	0.018	0.020	0.17	0.19	98.3	98.1
2	0.05	0.0544	0.49	0.53	95.1	94.7
3	0.0937	0.1028	0.92	1.01	90.8	89.9
4	0.1173	0.128	1.13	1.26	88.7	87.4
5	0.1173	0.1632	1.54	1.61	84.6	83.9

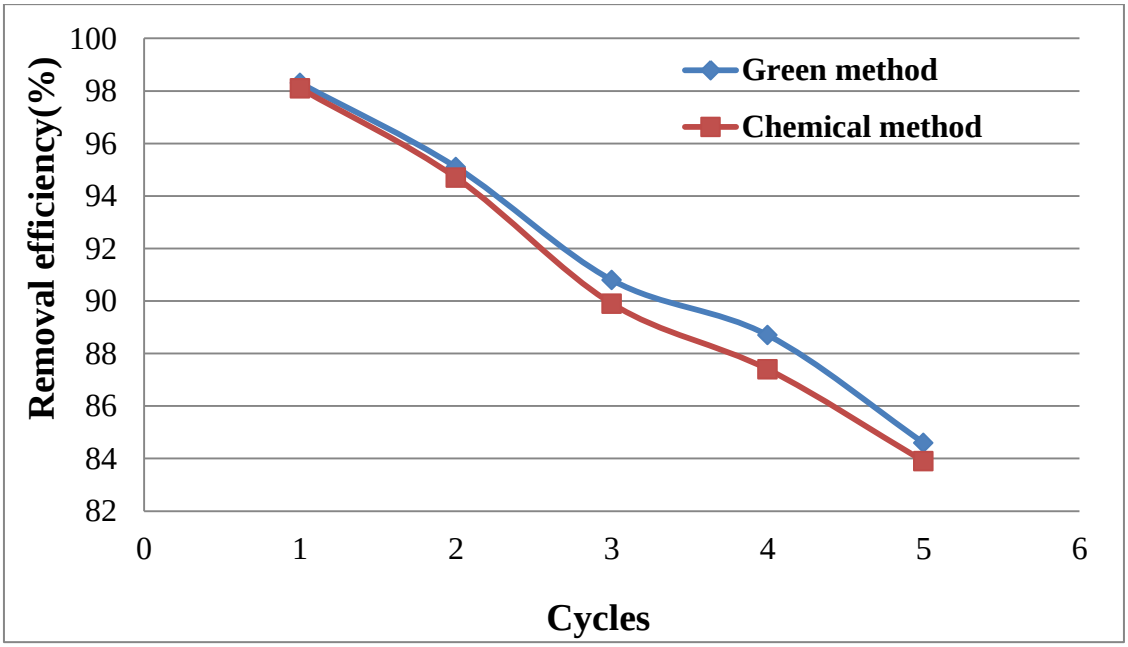

Figure 31: Reusability and regeneration of magnetite Fe_3O_4 adsorbent dosage 0.5 g, pH=9, time 60 min, and MB dye concentration = 50 mg/L.

CHAPTER FIVE

5. CONCLUSION AND RECOMMENDATION

5.1. Conclusion

Magnetite (Fe_3O_4) nanoparticles that were synthesized by chemical and green methods from *Prosopis julifera* as a reducing agent were prepared and characterized by different analytical methods. Different experimental conditions such as contact time, pH, initial adsorbate concentration, and adsorbent dose; to get optimum values of the mentioned parameters for the adsorption process were investigated. It was shown that the change in those parameters affects the adsorption process. The differential parameters of the process such as pH, the dose of adsorbent, initial concentration, and equilibrium time were optimized at 9, 0.5 g, 10 mg/L, and 60 min in both chemical and green methods, respectively for removal of MB dye even their removal efficiencies are different from each other. Maximum adsorption of 99.75 % and 99.505 % was obtained at 60 min, 10 mg/L of MB dye solution, and 0,5g of magnetite dose at room temperature with 150 rpm for green and chemical methods respectively. Keeping all parameters constant and increasing the initial concentration of MB dye in synthetic water from 10 mg/L to 50 mg/L, the percentage of removal efficiency of MB dye was decreased from 99.75 % to 94.899% and 99.505% to 94.21% for the green method and chemical method respectively. The data from kinetic experiments was found to fit well with the pseudo-second-order kinetic model with a high R^2 of 0.9999 and 0.9997 (green and chemical method respectively) value of than pseudo-first-order kinetic model which indicates the presence of chemisorption. The adsorption process of this research is well described by the Freundlich model than the Langmuir model. As the reusability test indicates magnetite nanoparticles can be used 98.3 to 84.6 and 98.1 to 83.9 from cycle 1 to cycle 5 for green and chemical methods respectively for the removal of methylene blue dye. These and the above results indicate that magnetite prepared that synthesized by the chemical and green method by using *Prosopis julifera* can be used for the removal of MB dye from aqueous solution even if their removal efficiency is different from each other. It has been found that greenly synthesized nanoparticles (GInPs) show high selectivity and adsorption capacities than chemical synthesized Fe_3O_4, to the removal of methylene blue from an aqueous solution.

5.2 Recommendation

This research study used synthetic methylene blue (MB) solution to avoid the influence of any other competitive substances on the adsorption process by Fe_3O_4 synthesized by a chemical and green method. Therefore, it is suggested to further evaluate the adsorption capability of the adsorbent by using effluents arising from municipal waste water. It is also possible to study the sorption thermodynamics of the system as well as desorption study to get a full picture of the removal capability of the biosynthesized Fe_3O_4 and Fe_3O_4 synthesized by chemical method for removal of methylene blue from different types of wastewater that contain MB from different industries like textile industries and compare the removal efficiency of MB from both water source by both methods. Other studies should be conducted on the effectiveness of the biological and synthesized Fe_3O_4 adsorbent in the removal of other pollutants like heavy metals that affect the environment and human health.

REFERENCES

Abou El-Nour, K.M.; Eftaiha, A.; Al. Warthan and A. Ammar., R.A. (2010). Synthesis and applications of silver Nanoparticles, *Arabian. Journal of Chemistry*. 135–140.

Aftabtalab, A. and Sadabadi, H. (2015). Application of Magnetite (Fe_3O_4) Nanoparticles in Hexavalent Chromium Adsorption from Aquatic Solutions, *J. Pet Environ Biotechnol.* 200.

Ahmad, A., Mohd-Setapar, S. H., Chuong, C. S., Khatoon, A., Wani, W. A., Kumar, R., & Rafatullah, M. (2015). Recent advances in new generation dye removal technologies: novel search for approaches to reprocess wastewater. *RSC advances*, *5*(39), 30801-30818.

Allen ON, Allen EK. The Leguminosae. (2009). A Source Book for Characteristics, Uses, and Nodulation. *The University of Wisconsin Press, Madison*, 1981.

Alventosa-deLara E, Barredo-Damas S, Alcaina-Miranda MI, Iborra- Clar MI (2012) Ultrafiltration technology with a ceramic mem- brane for reactive dye removal: optimization of membrane performance. *J Hazard Mate*r 209–210.

Ambashta RD, Sillanpää M.(2010) Water purification using magnetic assistance: a review. *J Hazardous Materials*, 38–49.

Arbabi, M.; Hematite, S.; Amiri, M. (2015). Removal of lead ions from industrial wastewater: A review of Removal methods. *International Journal of Epidemiology Resource*, 105–109.

Arabia.S.(2012). "ICP-OES Determination of Trace Metal Ions after Preconcentration Using Silica Gel Modified with 1, 2-Dihydroxyanthraquinone, 1007–1016.

Almaraz-Abarca N, Campos MG, Avila-Reyes JA, Naranjo-Jimenez N, Corral JH, Gonzalez-Valdez LS, (2007).*Journal of Food Composition and Analysis*,119.

Arokiyaraj, S., Saravanan, M., Prakash, N. U., Arasu, M. V., Vijayakumar, B. and Vincent, S.(2013).Enhanced antibacterial activity of iron oxide magnetic nanoparticles treated with Argemone Mexicana L. leaf extract: An in vitro study. *Materials Research Bulletin*, 3323–3327.

Barakat. M.A. (2011). New trends for removal of heavy metals from industrial wastewater. *Journal of Arabian chemistry*, 361-377.

Berihun. Y, & Solomon .D, (2017)"of Waste Resources Assessment of the Physicochemical and Heavy Metal Concentration from Effluents of Paint Industry in Addis Ababa, *Ethiopia*, 2252-5211.

Bhandari, Pragnesh N. Dave & Jaya. (2013). Prosopis julifera. *International Journal of Chemical Studies*, 2321-4902.

Boparai, H. K., Joseph, M., & Carroll, D. M. O. (2011). Kinetics and thermodynamics of cadmium ion removal by adsorption onto nano zerovalent iron particles. *Journal of Hazardous Materials*, 458–465.

Bruno Lellis, Cíntia Zani Fávaro-Polonio, João Alencar Pamphile and Julio Cesar Polonio. (2019).Effects of textile dyes on health and the environment and bioremediation potential of living organisms. *Biotechnology Research and Innovation*, 1-16.

Bulgariu, L., Escudero, L. B., Bello, O. S., Iqbal, M., Nisar, J., Adegoke, K. A., . . . Anastopoulos, I. (2019). The utilization of leaf-based adsorbents for dyes removal: A review. *Journal of Molecular Liquids, 276*, 728-747.

Cao M, Li Z, Wang J, Ge W, Yue T, Li R, Colvin V L and Yu W. (2012). Food related applications of magnetic iron oxide nanoparticles: enzyme immobilization, protein purification, and food analysis Trend. *Food Science and Technology*, 27- 47.

Carrott PJM, Carrott MMLR, Roberts RA (1991) Physical adsorption of gases by microporous carbons. Colloids Surf 58:385–400

Cheng. F, J. W. Betts, S. M. Kelly, J. Schaller, and T. Heinze, (2013). "Synthesis and antibacterial effects of aqueous colloidal solutions of silver nanoparticles using amino cellulose as a combined reducing and capping reagent," *Green Chemistry*, 989–998.

Cornell, RsM and Schwertmann U. (1996). The iron oxides. *VCH Press, Weinheim, Germany*, 573.

Djurisic, A.B.; Leung, Y.H.; Ng, A.M.C.; Xu, X.Y.; Lee, P.K.H.; Digger, N.; Wu, R.S.S.(2015) Toxicity of metal oxide nanoparticles: Mechanisms, characterization, and avoiding experimental artifacts. *Small*, 26–44.

Dökmeci. A.H. (2018). Toxicological- Environmental and Industrial-Disasters. *Nobel Tıp Kitabevi, Istanbul. Turkey*, 99-120.

Duffus. J.H. (2002). "Heavy metals" is a meaningless term. (IUPAC Technical Report). *Pure Applied Chemistry*, 793- 807.

Estelrich J, Escribano E, Queralt J, Busquets MA. (2015). Iron oxide nanoparticles for magnetically-guided and magnetically-responsive drug delivery. *International Journal of Molecular Sci*ence, 8070–8101.

Eunice Aparecida Campos,Denise Villela Barcza Stockler Pinto, José Irineu Sampaio de Oliveira. (2015). Synthesis, Characterization, and Applications of Iron Oxide Nanoparticles. *Aerosp. Technological Management, São José dos Campos*, 267-276.

Felker, P. 2005. Mesquite Flour: New Life for an Ancient Staple. Gastronomica: *The Journal of Food and Culture*, 85-89.

Fu, P., Lin, X., & Chen, Z. (2018). Porous Fe 0/C magnetite for removal of aqueous Pb (ii) ions: equilibrium, long-term performance, and mechanism studies. *RSC advances*, *8*(45), 25445-25455.

García-Montaño J, Domènech X, García-Hortal JA, et al (2008) The testing of several biological and chemical coupled treatments for Cibacron Red FN-R azo dye removal. J Hazard Mater 154:484– 49

Ge.F, Li.M.M, Ye.H, Zhao.B.X. (2012). effective removal of heavy metal ions Cadmium, Zinc, Lead, and Cupper from aqua solution by polymer-modified magnetic nanoparticles. *journal of hazard materials*, 366-372.

George William Kajjumba, S. E. (2018). Modeling of Adsorption Kinetic Processes—Errors, Theory, and Application. In S. Edebali, Advanced Sorption Process Applications Selçuk University, *Turkey: Intech Open publisher*, 1-20.

Girmaye. B,(2014) "Assessment of heavy metals in vegetables irrigated with Awash River in selected farms around Adama, 428–434.

Gotic, M., Jurkin, T., Music, S., (2009). Iron (III) precursor to magnetite and vice versa. *Mater. Resear. Bulletin*, 44, 2014-2021.

Handan Dökmeci, A. (2020). Environmental Impacts of Heavy Metals and their Bioremediation. *In technological Open*, 1-18.

Hemingway BS. (1990). Thermodynamic properties for bunsenite, NiO, magnetite, Fe3O4 and hematite, Fe2O3 with comments on selected oxygen buffer reactions. *American Mineralogist* .781-790.

Heuze, V.,s G. Tran, M. Boval and D. Renaudeau. (2011). Mesquite (Prosopis juliflora). Feedipedia. org and Tables Regions Chaudes. A project by *INRA, CIRAD, and AFZ with the support of FAO*. 15.

Holzwarth, U., & Gibson, N. (2011). The Scherrer equation versus the " Debye – Scherrer equation ," 6 *(SEPTEMBER)*, 21027.

Hosseini Koupaie E, Alavi Moghaddam MR, Hashemi SH (2011) Post-treatment of anaerobically degraded azo dye Acid Red 18 using aerobic moving bed biofilm process: enhanced removal of aromatic amines. *J Hazard Mater*, 147–154.

Jiang, Wu, W.; He, Q.G.; C.Z. (2008). Magnetic iron oxide nanoparticles: Synthesis and surface fictionalizations strategies, *Nanoscale, Res. Lett*., 397–415.

Jianlong Wang, X. G. (2020). Adsorption isotherm models: Classification, physical meaning, application, and solving method. Chemosphere 258 127279, 3-22.

Kadirvelu.K, Thamariaselvi.K and Namasivayam.C. (2001). Removal of heavy metals from industrial wastewater by adsorption onto activated carbon prepared from agricultural solid waste. *Biological resource technology*, 63-65.

Kandasamy, J., Vigneswaran, S., Hoang, T., & Chaudhary, D. (2009). Adsorption and biological filtration in wastewater treatment. *Water and Wastewater Treatment Technologies, EOLSS and UNESCO, Oxford, United Kingdom*, 173-204.

Karthik, V et al. (2020). Composite, Comparative, and Equilibrium Studies on Anionic and Cationic Dyes Removal by Nano-Alumina-Doped Catechol Formaldehyde. *Journal of Chemistry*, 1-15,

Kaul, R., Kumar, P., Burman, U., Joshi, P., Agrawal, A., Raliya, R., et al. (2012). Magnesium and Iron Nanoparticles Production Using Microorganisms and Various Salts. *Material Science-Poland*, 254–258.

Khalid Z. Elwakeel ORCID, Ahmed M. Elgarahy, Ziya A. Khan, Muath S. Almughamisi and Abdullah S. Al-Bogam. (2020). Perspectives regarding metal/mineral-incorporating materials for water purification. *Material Advance*, 1546-1574.

Khamparia, S., & Jaspal, D. K. (2017). Adsorption in combination with ozonation for the treatment of textile wastewater: a critical review. *Frontiers of Environmental Science & Engineering*, 8.

Khayat Sarkar, Z.; Khayat Sarkar, F.(2013). Selective removal of lead (II) ion from wastewater using superparamagnetic monodispersed iron oxide (Fe_3O4_4) nanoparticles as an effective adsorbent. *International journal of nanoscience and Nanotesschnology*.109–114.

Kheddo, A., Rhyman, L., Elzagheid, M. I., Jeetah, P., & Ramasami, P. (2020). Adsorption of synthetic dyed wastewater using activated carbon from rice husk. *SN Applied Sciences*, 1-14.

Krafts. K, &. H. (2012). A. Sko ´risk-Stania, From methylene blue to chloroquine: a brief review of the development of antimalarial therapy. *Parasitology Resource*, 1–6.

Krishnaraj .C, Ramachandran .R, Mohan .K and Kalaichelvan .P.T. (2012). importance of nanomaterials for industrial wastewater treatment. *Korean Journal of Chemical Engineering*, 95.

Kumar, V. G, and Ananthu A. Prem. (2018). Green synthesis and characterization of iron oxide nanoparticles using Phyllanthus Niruri extract, *Oriental Journal of Chemistry*, 2583-2589.

Kurniawan.T.S, Chan.G.Y.S, Lo.W.H, Babel.S. (2006). physio-chemical treatment techniques for wastewater laden with heavy metals. *Chemical engineering*, 83-98.

Kyzas, G. Z., & Kostoglou, M. (2014). Green adsorbents for wastewaters: a critical review. *Materials*, 333-364.

Laurent .S, Forge.D, Port .M et al. (2008). Magnetic iron oxide nanoparticles: synthesis, stabilization, vectorization, physicochemical characterizations, and biological application. *Magnetic iron oxide nanoparticles: synthesis, stabilization, vectorization, physic Chemical Reviews, physical-chemical*, 2110.

Madan Singha, M. G. (2018). Size and shape effects on the band gap of semiconductor compound nanomaterials. *Journal of Taibah University for Science*, 1-7.

Mahmoudi.M, S. W. (2011). "Superparamagnetic iron oxide nanoparticles (SPIONs): development, surface modification, and applications in chemotherapy. *Advanced Drug Delivery Reviews*, 24 - 46.

Malihe Pooresmaeil, H. N. (2020). Chapter 14 - Application of polysaccharide-based hydrogels for water treatments. In Y. Chen, Hydrogels Based on Natural Polymers. *Elsevier*, 411-455

Manc.V.S & Babu.P.V.V. (2011). Studies on the adsorption of Brilliant Green dye from aqueous solution onto low-cost NaOH treated sawdust. *Desalination*, 321-329.

Mauremootoo, R. 2006. *Biocontrol News and Information.* 37-40.

Milonjić SK, Kopečni MM, Ilić ZE (1983) The point of zero charge and adsorption properties of natural magnetite. *Journal of Radioanalytical Chemistry*, 15–24.

Mittal, A.K., Chisti, Y. and Banerjee, U.C. (2013) Synthesis of Metallic Nanoparticles Using Plant extracts, I*nternational Biotechnology Advances*, 346-356.

Muhammad Ibrahim, Muhammad Nadir, Amanat Alii. (2013). phytochemical of Prosopis juliflora. *Department of Chemistry, University of Karachi, Karachi, Pakistan*, 2101-2104.

Mulana, F., Djuned, F. M., Fadli, M., & Meilian, M. (2020). Fabrication of Activated Charcoal from Coconut Shell Combined with Coal Fly Ash from PLTU Nagan Raya for Adsorption of Methylene Blue. *Paper presented at the IOP Conference Series: Materials Science and Engineering*.

Nagajhoti.P.C, Lee.K.D, Sreekanth.T.V.M. (2010). Heavy metals, occurrence, and toxicity for the plant. *A review, Environmental Chemical Lettice*, 199-216.

Nakajima.A & Baba, Y. (2004). Mechanism of hexavalent chromium adsorption by persimmon tannin. *Water resource*, 2859-2864.

Nasr, J. B., Hamdi, N., & Elhalouani, F. (2017). Characterization of activated carbon prepared from sludge paper for methylene blue adsorption. *JMES, 8*, 1960-1967.

Nriagu, J. 0. and Pacyna, J. M. (1988). Quantitative assessment of worldwide contamination of air, water and soils by trace metals., 134–139.

Nurbas, M., Ghorbanpoor, H. and Avci, H.(2017) . An eco-friendly approach to synthesis and characterization of magnetite (Fe3O4) nanoparticles using Platanus Orientalis l. Leaf extract, Digestion. *Journal of Nanomaterials and Biostructures*, 993 - 1000.

Oana Stoian , Cristina Ileana Covaliu , Gigel Paraschiv , Gina-Alina Catrina (Traistaru) , Mihai Nit ,ă-Lazăr , Ecaterina Matei , Sorin S , tefan Biris ,and Paula Tudor . (2021). Magnetite Oxide Nanomaterial Used for Lead Ions Removal from Industrial Wastewater. *Materials* , 14.

Oswald.M, Aroua. M.K, Daud. W.A.W, Baroutian.S. (2009). Removal of hexavalent chromium contaminated water and wastewater. *Review on, Water, Air and soil pollutant*, 59-77.

Padmavathy, K.S., Madhu, G., Haseena. P.V.,(**2016**).Effects of pH, adsorbent dosage, time, initial concentration, and adsorption isotherm study for the removal of hexavalent chromium (Cr (VI)) from wastewater by magnetite nanoparticles. *Int. Conf. Eng. Sci. Techno*, 24, 585-594.

Pattanayak, M. and Nayak, P.L. (2013) 'Green synthesis and characterization of zero-valent iron nanoparticles from the leaf extract of Azadirachta indica (Neem)', *World Journal of Nano Science & Technology*, .06–09

Patterson, J. W. (1985). Industrial Wastewater Treaûnent Technology. 2nd edition, Butterworth Publishers, Stoneham, MA, USA.

Petrova. P, Karadjova. I, Chochkova .M, Dakova .I, and Karadjov, M. (2017). New amino acid-modified silica gel sorbents for solid phase extraction of Au (III). 95–100.

Pilli S, Bhunia P, Song Y, LeBlanc RJ, Tyagi RD, Surampalli RY. (2011). Ultrasonic pretreatment of sludge. *A review Ultrasonic Sonochemical*, 1-18.

Pradeep.T. (2009). Noble metal nanoparticle for water purification. *critical review, thin solid films*, 6441-6478.

Rajabi, M., Mahanpoor, K., & Moradi, O. (2017). Removal of dye molecules from aqueous solution by carbon nanotubes and carbon nanotube functional groups: a critical review. *RSC Advances*, *7*(74), 47083-47090.

Ramachandran, P., Vairamuthu, R., & Ponnusamy, S. (2011). Adsorption isotherms, kinetics, thermodynamics, and desorption studies of reactive Orange 16 on activated carbon derived from Ananas comosus (L.) carbon. *Journal of Engineering and Applied Sciences*, *6*(11), 15-26.

Rauwel. P, Küünal. S, Ferdov. S, and Rauwel. E . (2015). A Review on the green Synthesis of Silver Nanoparticles and Their Morphologies Studied via TEM. *Advanced Materials Science Engineering*, 1–9.

Registry. (ATSDR), United States Agency for Toxic Substances and Disease. (2019). Toxicological Profile for Lead (Draft for Public Comment). *Department of Health and Human Services Atlanta, GA, USA*, 582.

Rodriguez, R. C. (2015). Removal of lead, chromium, and cadmium from wastewater. *Deppartement of Enginyeria Quimica*, 1-162.

Sabah Mohamed Abdelbasir & Ahmed Esmail Shalan. (2019). nanomaterials for industrial wastewater treatment. *Korean Journal of Chemical Engineering*, 36-38.

Sabzoi Nizamuddin, Siddiqui. M.T.H, Mubarak. N.M, Humair Ahmed Baloch, Abdullah . E.C, Shaukat Mazari§ .A, Griffin . G.I, Srinivasan. M.P, Akshat Tanksale. (2019). Iron oxide nanomaterials for removal of heavy metals and dyes from wastewater. *Nanoscale Materials in Water Purification*, 1-27.

Samsami, S., Mohamadizaniani, M., Sarrafzadeh, M.-H., Rene, E. R., & Firoozbahr, M. (2020). Recent advances in the treatment of dye-containing wastewater from textile industries: Overview and perspectives. *Process safety and environmental protection, 143*, 138-163.

Sarkar S, Ponce NT, Banerjee A, et al (2020) Green polymeric nano-materials for the photocatalytic degradation of dyes: a review. *Environ Chem* Lett 18:1569–1580.

Sartape, A. S., Mandhare, A. M., Jadhav, V. V., Raut, P. D., Anuse, M. A., & Kolekar, S. S. (2017). Removal of malachite green dye from aqueous solution with adsorption technique using Limonia acidissima (wood apple) shell as low-cost adsorbent. *Arabian Journal of Chemistry, 10*, S3229-S3238.

Sen Gupta.S & Bahattarchyya.K.G. (2011). Kinetics of adsorption of metal ions from aqua on inorganic materials. *Advance colloidal interface science,* 39-55.

SHI, H.-c. (2000). Industrial wastewater types, amounts, and effects. *Department of Environmental Science and Engineering, Tsinghua University, Beijing, China*, 1-5.

Singh. J, Dutta. T, Kim. K. H, Rawat. M, Samddar. P, and Kumar. P. (2018). 'Green'synthesis of Metals and Their Oxide Nanoparticles: Applications for Environmental Remediation. *journal of nanobiotechnology*, 84.

Singh.R, Bhatia .R &. (2020). A review on nanotechnological application of magnetic iron oxides for heavy metal removal. *Journal of Water Process Engineering*, 100845.

Smith, B., (1998). Infrared spectral interpretation. *System. Appro.3*, 4-78.

Sun A., Wu S., Zhai F, J. Wang. (2011). Fe_3O_4 magnetic nanoparticles synthesis from tailings by ultrasonic chemical co-precipitation, *Material Lettice*, 1882–1884.

Sun, D., Zhang, Z., Wang, M., & Wu, Y. (2013). Adsorption of reactive dyes on activated carbon developed from *Enteromorpha prolifera.*

Surendhiran D, Sirajunnisa A, Tamilselvam K (2017) Silver–magnetic nanocomposites for water purification. *Environ Chem Lett 15:367–386*

Tamene.F. (2008) February, "Faculty of Science,".

Teja AS. and Koh, PY. (2009). Synthesis, properties, and applications of magnetic iron oxide nanoparticles, Progress in Crystal Growth and Characterization of Materials, 22-45.

Yang L. (2008). Development of receptor-targeted magnetic iron oxide nanoparticles for efficient drug delivery and tumor imaging, Journal of Biomedical Nanotechnology, 439.

Yagub, M. T., Sen, T. K., Afroze, S., & Ang, H. M. (2014). Dye and its removal from aqueous solution by adsorption: a review. *Advances in colloid and interface science*, 172-184.

Yu, L., Wang, J., & Gong, P. (2013). Improving 30 m global land-cover map FROM-GLC with time series MODIS and auxiliary data sets: a segmentation-based approach. *International Journal of Remote Sensing, 34*(16), 5851-5867.

Yuan, N., Cai, H., Liu, T., Huang, Q., & Zhang, X. (2019). Adsorptive removal of methylene blue from aqueous solution using coal fly ash-derived mesoporous silica material. *Adsorption Science & Technology, 37*(3-4), 333-348.

Yunusa, U., & Ibrahim, M. (2019). Reclamation of malachite green-bearing wastewater using desert date seed shell: adsorption isotherms, desorption and reusability studies. *Chemsearch Journal, 10*(2), 112-122.

Wan Ngah.W.S and Hafiah.M.A.K.M. (2008). Removal of heavy metal ions from wastewater by chemically modified plant wastes as adsorbent. *Biological resource technology*. 3935-3948.

Weldegebriel .Y, Chandravanshi.B.S, and Wondimu.T. (2012). Concentration levels of metals in vegetables grown in soils irrigated with river water in Addis Ababa, Ethiopia. *Ecotoxicology and Environmental Safety*, 57–63.

Witt, A. (2010). Biofuels and Invasive Species from an African Perspective-a Review. GCB *Bioenergy*. 2:321-329.

Wu W, He, Q and Jiang C. (2009). Magnetic iron oxide nanoparticles: synthesis and surface functionalization strategies. *Chemical Inform*ation, 1.

Yeshiwas. Y and Tadele. E, (2017). Review on Heavy Metal Contamination in Vegetables Grown in Ethiopia and Its Economic Welfare Implications," *Journal of Biological Agricultural Healthcare*, 31–44.

Yetter, AR. Risha, GA. and Son, SA . (2009). Metal particle combustion and nanotechnology, *P . Combust Inst,*1819-1838.

Ziemniak SE, Jones ME, Combs KES (1995) Magnetite solubility and phase stability in alkaline media at elevated temperatures. *Journal of Solution Chemistry*, 837–877

Zhang, J.; Lin, S.; Han, M.; Su, Q.; Xia, L.; Hui, Z.(2020) Adsorption properties of magnetic magnetite nanoparticle for coexistent Cr (VI) and Cu (II) in the mixed solution. *Water*, 446.

Zhang, S., Tao, L., Zhang, Y., Wang, Z., Gou, G., Jiang, M., . . . Zhou, Z. (2016). The role and mechanism of K2CO3 and Fe3O4 in the preparation of magnetic peanut shell-based activated carbon. *Powder Technology, 295*, 152-160.

Zhang, Y., Jin, F., Shen, Z., Wang, F., Lynch, R., & Al-Tabbaa, A. (2019). Adsorption of methyl tert-butyl ether (MTBE) onto ZSM-5 zeolite: Fixed-bed column tests, breakthrough curve modeling, and regeneration. *Chemosphere, 220*, 422-431.